JOURNAL OF AGRICULTURAL AND FOOD CHEMISTRY

pubs.acs.org/JAFC Article

Linolenic Acid-Derived Oxylipins Inhibit Aflatoxin Biosynthesis in *Aspergillus flavus* through Activation of Imizoquin Biosynthesis

Shaowen Wu, Qunjie Zhang, Wenyang Zhang, Wenjie Huang, Qian Kong, Qinjian Liu, Wenyan Li, Xinlu Zou, Chun-Ming Liu, and Shijuan Yan*

Cite This: https://doi.org/10.1021/acs.jafc.2c06230 Read Online

ACCESS | Metrics & More | Article Recommendations | Supporting Information

ABSTRACT: Oxylipins play important signaling roles in aflatoxin (AF) biosynthesis in *Aspergillus flavus*. We previously showed that exogenous supply of autoxidated linolenic acid (AL) inhibited AF biosynthesis in *A. flavus* via oxylipins, but the molecular mechanism is still unknown. Here, we performed multiomics analyses of *A. flavus* grown in media with or without AL. Targeted metabolite analyses and quantitative reverse transcription (qRT)-polymerase chain reaction (PCR) showed that the imizoquin (IMQ) biosynthetic pathway was distinctly upregulated in the presence of AL. ^{13}C-glucose labeling confirmed in parallel that the tricarboxylic acid cycle was also enhanced by AL, consistent with observed increases in mycelial growth. Moreover, we integrated thermal proteome profiling and molecular dynamics simulations to identify a potential receptor of AL; AL was found to interact with a transporter (ImqJ) located in the IMQ gene cluster, primarily through hydrophobic interactions. Further analyses of strains with an IMQ pathway transcription factor overexpressed or knocked out confirmed that this pathway was critical for AL-mediated inhibition of AF biosynthesis. Comparison of 22 assembled *A. flavus* and *Aspergillus oryzae* genomes showed that genes involved in the IMQ pathway were positively selected in *A. oryzae*. Taken together, the results of our study provide novel insights into oxylipin-mediated regulation of AF biosynthesis and suggest potential methods for preventing AF contamination of crops.

KEYWORDS: *Aspergillus flavus, aflatoxins, imizoquin, multiomics, thermal proteome profiling*

INTRODUCTION

Aspergillus flavus is a filamentous fungus notorious for causing invasive and noninvasive aspergillosis in many species, including in insects, humans, and other animals.[1] *A. flavus* produces potent naturally carcinogenic and toxic compounds, aflatoxins (AFs), primarily in the forms of B1, B2, G1, and G2; these toxins contaminate a broad range of oil-rich crops, such as corn, peanuts, walnuts, and sunflower.[1,2] Humans and other animals suffer from a variety of diseases (e.g., cancers, infertility, and immune suppression) after ingesting AF-contaminated food or feed.[3] Crop infections with *A. flavus* also cause huge economic losses worldwide. Exploring the key factors in AF biosynthetic regulation, especially inhibition, is essential for formulating effective biological prevention and control strategies.

The genes involved in AF biosynthesis form a cluster, including at least 30 metabolic genes and two transcriptional regulators (*aflR* and *aflS*), which coordinate the expression of metabolic genes.[3] Previous studies have shown that there are at least 12 genes that negatively regulate AF biosynthesis, such as *gprA*, *msnA*, *ppoC*, *lox*, and *fadA*, and 39 genes that positively regulate it, such as *aflR*, *aflS*, *nsdC*, *creA*, *hbx1*, *pbsB*, *laeA*, and *veA*.[4] These genes are involved in cell signaling, reproductive processes, growing conditions, and oxidative stress responses.[3] For example, gene *laeA* plays distinct roles in the development and pathogenesis of *A. flavus*, its deletion reduced *aflR*, *aflD*, and *aflS* mRNA levels and inhibited AF production.[5] Gene *veA* regulates the synthesis of multiple mycotoxins in *A. flavus*, including AFs.[6] A subunit of the G-protein signaling pathway, *fadA*, regulates several genes, such as *pkaA*, *brlA*, *aflT*, and *aflR*, and governs both AF and sterigmatocystin biosynthesis.[3] In addition, the antioxidant-related catalase CTA1 and a putative phosphatase, Ssu72, regulate the development and AF biosynthesis in *A. flavus*.[7,8] These studies suggest that AF biosynthesis is regulated by a complex gene network.

Several small molecular compounds, such as polyphenols, benzimidazole derivatives, fatty acids (FAs), and oxylipins, have also been shown to regulate AF biosynthesis.[9−12] Specifically, gallic acid, 5-azacytidine, stearic acid (SA), oleic acid, linoleic acid, 13(*S*)-hydroperoxy-9,11-octadecatrienoic acid (13(*S*)-HPODE), and 13(*S*)-hydroperoxy-9,11,15-octadecatrienoic acid (13(*S*)-HPOTE) inhibit AF biosynthesis, whereas myristic acid, palmitic acid, and 9(*S*)-HPODE promote it.[13−18] In studying the effects of FAs on AF biosynthesis, we previously showed that both saturated and unsaturated FAs promote AF production, but that autoxidated polyunsaturated FAs, especially autoxidated linolenic acid (AL), inhibit AF production via oxylipins.[19] G-protein-coupled receptors (GPCRs) and related signaling pathways are involved in oxylipin-mediated regulation of AF biosynthesis. *A. flavus* strains with mutations in GPCRs revealed that there

Received: September 7, 2022
Revised: November 24, 2022
Accepted: November 30, 2022

was no conidiation response to 13(*S*)-HPODE treatment, and a structural analog of 9(*S*)-HPODE was shown to bind to the mammalian GPCR G2A.[20,21] However, the details of the mechanism by which oxylipins regulate AF biosynthesis remain largely unclear.

We previously reported that exogenous application of AL inhibits AF biosynthesis in *A. flavus* via oxylipins. To elucidate the underlying mechanism of this inhibition, we here conducted comprehensive multiomics analyses, molecular dynamics (MD) simulations, and functional validations. The results showed that AL activated the imizoquin (IMQ) biosynthetic pathway and enhanced tricarboxylic acid (TCA) cycling. We also showed that AL interacted with the transporter ImqJ, which is encoded by a gene in the IMQ gene cluster. We demonstrated that activation of the IMQ pathway was critical for AL-mediated inhibition of AF biosynthesis. Furthermore, a comparison of 22 assembled *A. flavus* and *Aspergillus oryzae* genomes revealed that genes involved in the IMQ pathway were positively selected in *A. oryzae*.

MATERIALS AND METHODS

Fungal Strains and Biochemical Experiments. *A. flavus* strain A3.2890 was obtained from the China General Microbiological Culture Collection Center at the Institute of Microbiology, Chinese Academy of Sciences.[19,22] The NRRL 3357 strain was obtained from the United States Department of Agriculture Agricultural Research Service (USDA-ARS) (Peoria, IL). Strains ΔimqK and OE::imqK, which were engineered from the NRRL 3357 strain, were obtained from Professor Nancy P. Keller; details about these strains have previously been reported in ref 23. The NRRL 3357 strain was used to compare physiological phenotypes and differences in metabolite content between strains ΔimqK and OE::imqK. The A3.2890 strain was used for all other experiments, including transcriptomics, quantitative reverse transcription (qRT)-polymerase chain reaction (PCR), gas chromatography-mass spectrometry (GC-MS)- and liquid chromatography-mass spectrometry (LC-MS)-based metabolomics, lipidomics, proteomics, thermal proteome profiling (TPP) assay, and metabolic flux experiments, except where otherwise specified. For the fatty acid treatment experiments, stearic acid (C18:0, catalog number S4751) and linolenic acid (C18:3, catalog number 62160) were purchased from Sigma-Aldrich (St. Louis), with purities above 99 and 98.5%, respectively. The 250 mM linolenic acid or stearic acid stock solutions were prepared by dissolving them in ethanol, respectively; 200 μL of linolenic acid, stearic acid stock solution, or ethanol alone as control was transferred to conical flasks, and these flasks were then placed in a laminar flow cabinet for 4 h to allow the ethanol to evaporate completely. These three experimental conditions were described as AL, SA, and CK, respectively. AL was obtained after linolenic acid autoxidation during 4 h air drying. As characterized previously, AL was a mixture of different oxylipins without residual linolenic acid,[19] which included 10.1% 9,14-diHPOTE, 10.6% 9,15-diHPOTE, 16.8% 9,16-diHPOTE, 11.3% 13,16-diHPOTE, 2.7% 9,11-diHPOTE, 43.8% 9-HPOTE, 2.3% 13-HPOTE, and 2.4% 17-HPOTE. Eighteen milliliter of liquid glucose mineral salt (GMS) medium and 2 mL of spore suspension were added to each flask and cultured, as previously described,[22] with an initial density of 0.8×10^6 spores/mL. All GMS liquid cultures were grown in continuous darkness by shaking at 180 rpm and 28 °C.[19] Dry weight measurements and measurements of glucose, kojic acid, and aflatoxins were performed as previously described.[19] The NH_4^+ content in growth media was measured using a Multi N/C (2100 S) analyzer.[24]

Scanning Electron Microscopy. One-day-old mycelial samples were fixed with 2.5% (v/v) glutaraldehyde at 4 °C overnight and then washed as previously reported.[25] Fixed samples were dehydrated with a gradient ethanol series (30, 50, 70, 75, 80, 90, 95, and 100%) and then incubated in 100% ethanol. Specimens were then dried via critical-point drying in CO_2 and coated with gold. Fungal morphologies were then observed at different magnifications using a scanning electron microscope (S-3400N, HITACHI, Japan) at 15.0 kV.

Transcriptomics. After incubation for 1, 2, and 3 days, the mycelial samples of *A. flavus* were collected and then immediately frozen in liquid nitrogen. There were three biological replicates for each sample. Total RNAs of CK and AL mycelial samples were extracted using the TaKaRa MiniBEST Plant RNA Extraction Kit (TaKaRa, Japan), according to the manufacturer's instructions. The total RNA was then purified using an Epicentre Ribo-zerorRNA Removal Kit (Epicentre). Transcriptome libraries were constructed using the rRNA-depleted RNA by NEBNext Ultra Directional RNA Library Prep Kit for Illumina (NEB), following the manufacturer's instructions. The resulting libraries were sequenced on an Illumina HiSeq. 4000 to generate paired-end reads 150 nucleotides in length. Reads of low quality (phred score <30) or short length (<40 bp) were trimmed using Trimmomatic.[26] A total of 32.5 million trimmed, paired, and size-filtered reads were used in transcriptome assembly. The *A. flavus* NRRL 3357 genomic sequence and annotations (assembly JCVI-afl1-v2.0) were downloaded from NCBI (http://www.ncbi.nlm.nih.gov). The index of the reference genome was built using Bowtie (v2.2.3),[27] and the clean paired-end reads were aligned to the reference genome using TopHat (v2.0.13).[28] We compared the expression variance during mycelia growth by the growth specificity index (gsi), which refers to the algorithm for tissue specificity index τ as below[29]

$$\tau = \frac{\sum_i^N \left(1 - \frac{x_i}{x_{\max}}\right)}{N - 1}$$

where x_i is the gene expression for different growth time points i, $x_{\max}$ is the maximum gene expression, and N is the number for the growth time point. Further details on measuring and comparing the gene expression levels, differentially expressed genes (DEGs), and the Kyoto Encyclopedia of Genes and Genomes (KEGG) biochemical pathway analysis are included in the Supporting Information.

Gas Chromatography (GC)-Mass Spectroscopy (MS)-, and Liquid Chromatography (LC)-MS-Based Metabolomics. Metabolomes were analyzed for CK and AL mycelial samples grown for 1, 2, and 3 days. There were four biological replicates for each sample. Metabolites were extracted from fresh samples as previously described.[30] For primary metabolite profiling, a dried 150 μL aliquot from the lower phase was derivatized using *N*-methyl-*N*-(trimethylsilyl) trifluoroacetamide and analyzed by GC-MS (7890A-5975C, Agilent Technologies Inc., Santa Clara, CA) as previously described.[31] For specialized metabolite profiling, another dried 150 μL aliquot from the lower phase was resuspended in 150 μL of a 1:1 (v/v) mixture of water and ultra-performance liquid chromatography (UPLC)-grade methanol and then analyzed using an LC-MS system equipped with reversed-phase liquid chromatography (RPLC) (Dionex, Thermo Fisher Scientific, San Jose, CA) and a high-resolution Orbitrap Fusion MS system (Thermo Fisher Scientific) as described in our previous work.[32]

LC-MS-Based Lipidomics. Lipidomes were analyzed for CK and AL mycelial samples grown for 1, 2, and 3 days. There were four biological replicates for each sample. A dried aliquot from the upper phase of the system described in Gas Chromatography(GC)-Mass Spectroscopy (MS)-, and Liquid Chromatography (LC)-MS-Based Metabolomics section was resuspended in 200 μL of UPLC-grade ACN/2-propanol/dichloromethane (1:1:1, v/v/v) and then analyzed using an LC-MS system equipped with RPLC (Dionex, Thermo Fisher Scientific, San Jose, CA) and a high-resolution Orbitrap Fusion MS system (Thermo Fisher Scientific, San Jose, CA) as described in our previous work.[32]

Proteomics Using nanoLC-MS. The proteomics was analyzed for CK and AL mycelial samples grown for 3 days. There were three biological replicates for each sample. Proteins were extracted from fresh mycelia by grinding 0.2 g per sample in 1 mL of extraction buffer, as previously described,[33] and then protein extraction, trypsin

https://doi.org/10.1021/acs.jafc.2c06230
J. Agric. Food Chem. XXXX, XXX, XXX−XXX

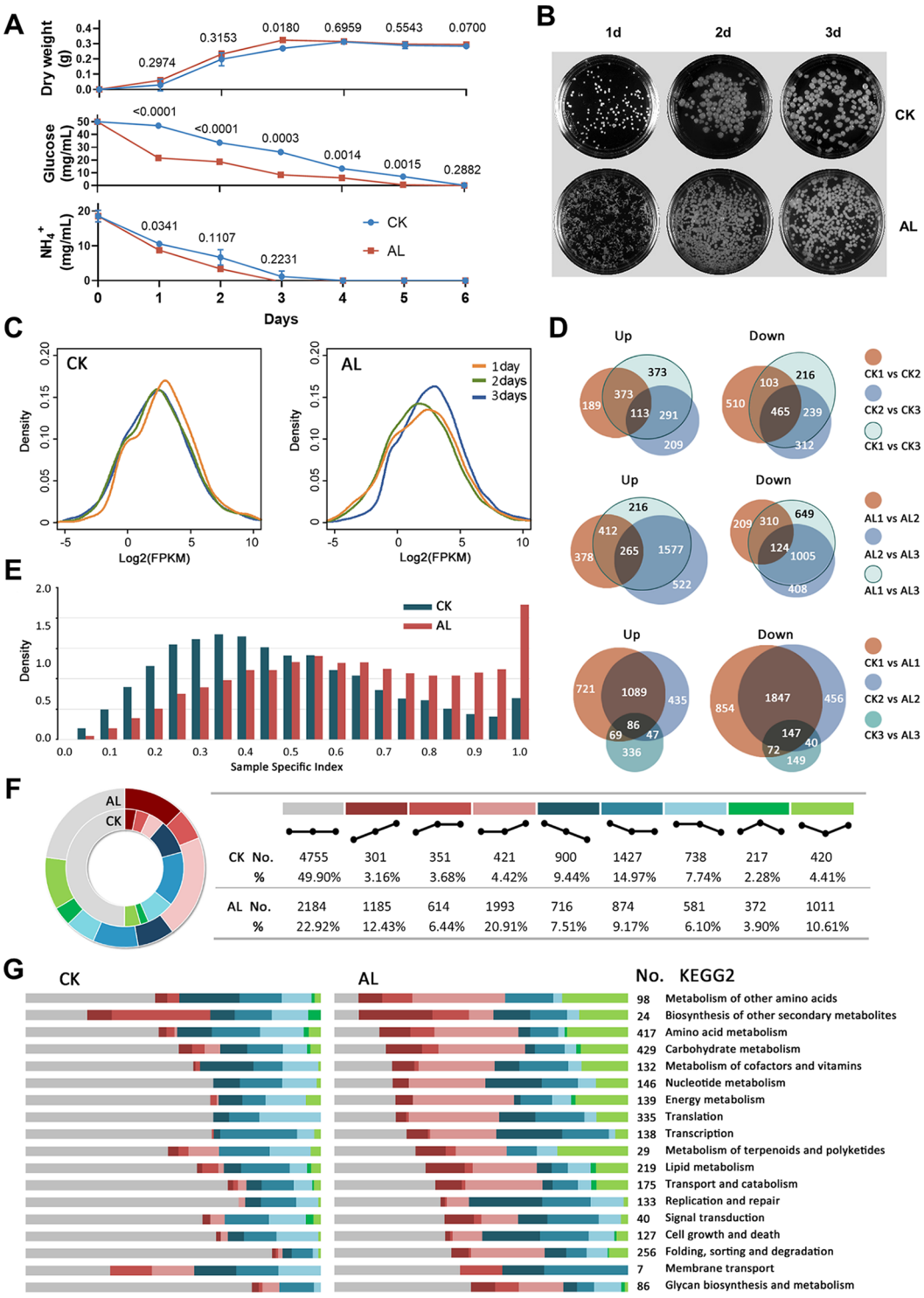

Figure 1. Autoxidated linolenic acid (AL) treatment altered the morphology and transcriptome of *A. flavus*. (A) Mycelia dry weight, glucose content in growth media, and NH_4^+ content in growth media over 6 days. The *p*-values obtained from the Student's *t*-test analysis of the data collected from each time point were presented. (B) Morphological changes in AL-treated and control (CK) mycelia over 3 days. (C) Distribution of gene expression levels in CK- and AL-treated mycelia. (D) Comparison of upregulated genes (up) and downregulated genes (down) between CK mycelia on different days (top row), between AL-treated mycelia on different days (middle row), and between CK and AL-treated mycelia on each day (bottom row). CK1-3 and AL1-3 represent samples collected on days 1 through 3, respectively. (E) Growth specificity index (gsi) distribution. (F) Abundance model of mycelial growth over 3 days. (G) KEGG biochemical pathway enrichment analysis of differentially expressed genes.

digestion, TMT labeling, and other proteomics methods were performed as previously described.[34] All tandem mass spectrometry (MS/MS) data were analyzed using Mascot (Matrix Science, London, U.K.; version 2.5.1). Mascot was used to search the *A. flavus* proteome database (40 023 entries) with trypsin set as the digestion enzyme. The fragment ion mass tolerance was set to 0.020 Da and the parent

https://doi.org/10.1021/acs.jafc.2c06230
J. Agric. Food Chem. XXXX, XXX, XXX−XXX

ion tolerance to 8.0 ppm. Scaffold (version 4.7.2, Proteome Software Inc., Portland, OR) was used to validate the MS/MS-based peptide and protein identifications. The details of peptide identification, differentially expressed proteins, and KEGG biochemical pathway analysis are included in the Supporting Information.

Thermal Proteome Profiling Assay. Proteins were extracted from CK and AL mycelial samples grown for 1 day using a similar protocol to the one previously described.[35] Mycelial samples (1.8 g wet weight) were placed in 15 mL centrifuge tubes, then resuspended, and extracted in 3.75 mL of freshly prepared native lysis buffer (20 mM *N*-(2-hydroxyethyl)piperazine-*N*′-ethanesulfonic acid (HEPES), 150 mM KCl, and 10 mM $MgCl_2$ at pH 7.5). Protein samples (50 μg each) were heated at 28, 34, 40, 46, 52, 58, 64, and 70 °C. Further details are included in the Supporting Information. Two independent experiments were performed for both CK and AL samples. Data were analyzed using the thermal proteome profiling (TPP) package in R as previously described.[36] Target proteins were screened using the R^2 values from fitting the melting curve and the shift in melting points between CK and AL treatment samples. Interacting proteins were classified as those with $\Delta T_m > 10$ °C and R^2 values >0.95 from fitting all four melting curves in the two independent experiments.

Gene Expression via Quantitative Reverse Transcription PCR (qRT-PCR). Gene expression was measured in *A. flavus* samples grown for 1, 2, and 3 days via qRT-PCR. There were three biological replicates per sample. Total RNA was extracted from frozen mycelial samples that had grown for 1, 2, and 3 days in CK or AL- or SA-containing media using the TaKaRa MiniBEST Plant RNA Extraction Kit (TaKaRa, Japan), following the manufacturer's instructions. Complementary DNA (cDNA) was synthesized from 500 ng of total RNA per sample using a HiScript-II Q RT SuperMix for qPCR (+gDNA wiper) Kit (Vazyme, Biotech Co., China), following the manufacturer's instructions. qRT-PCR was then performed in technical triplicate using ChamQ SYBR qPCR Master Mix (Vazyme Biotech Co., China) in a CFX connect system (Bio-Rad). The specificity of amplification was confirmed based on the melting curve. Relative gene expression was calculated using the $2^{-\Delta\Delta CT}$ method[37] with β-tubulin used as the internal control.

Metabolic Flux Experiments. To perform metabolic flux experiments with ^{13}C labeling, mycelia were grown as described above.[22] After mycelia had grown for 1, 2, and 3 days, the GMS medium was discarded, and D-glucose-$^{13}C_6$ labeled GMS medium was added. Mycelia were then grown for another 1.5 or 6 h. After collection, samples were measured by GC-MS as described above. The data were further analyzed using CORRECTOR software.[38] There were two biological replicates of samples grown for 1 day and three biological replicates of samples grown for 2 or 3 days.

Evolutionary Genomic Analysis. We identified 1:1 orthologs in 22 strains, namely, 13 assembled *A. flavus* and nine *A. oryzae* genomes, respectively, which were downloaded from NCBI and AspGD[39] by OrthoMCL.[40] Molecular evolution was investigated among the protein-coding genes in the set of 1:1 orthologs present in all 22 strains. The details of orthologous gene identification and d*N*/d*S* calculations for protein-coding genes are included in the Supporting Information. MEGA v6[41] was used for phylogenetic tree construction from 4,543 orthologs. The likelihood ratio test (LRT) was conducted to identify genes under positive selection using two methods. First was a site model, which compares 1a (nearly neutral) against 2a (selected site)[42] at two degrees of freedom (df = 2). The critical values were 5.99 and 9.21 at 5 and 1% significance levels, respectively. Second were branch-site models, which compared the modified model A (model = 2, NSsites = 2) to the corresponding null model using a fixed ω2 value of 1 (fix_omega = 1 and omega = 1) at df = 1. The critical values were 2.71 and 5.41 at 5 and 1% significance levels, respectively.[43,44]

MD Simulations. The structure of ImqJ was obtained using ColabFold.[45,46] CHARMM-GUI was used to build the initial structures of MD simulation systems.[47,48] Three simulation systems ImqJ-AL5, ImqJ-AL7, and ImqJ-All AL were built to examine the interaction between ImqJ and AL under different conditions. Details of the preparation steps for the ImqJ and AL structures and the simulation systems are included in the Supporting Information. MD simulations were conducted in GROMACS 2020 using the all-atom CHARMM36m force field and the TIP3P water model.[49,50] Topology and parameter files for the AL molecules were generated with a CHARMM generalized force field (CGenFF).[51] The steepest descent algorithm was used for energy minimization for 50 000 steps and the system equilibration lasted 1 ns with constraints on the hydrogen bonds in the NPT ensemble.[52] The semi-isotropic Parrinello–Rahman method was used to maintain the pressure at 1 bar using the algorithm with a time constant of 5 ps, and the Nose–Hoover thermostat was used with a time constant of 1 ps was used to maintain a constant temperature of 303.15 K.[53,54] Trajectories were produced with constraints on the H-bonds and lasted 300, 300, and 500 ns for ImqJ-AL5, ImqJ-AL7, and ImqJ-All AL, respectively, for an aggregated time of 1.1 μs. H-bonds were constrained using the LINCS algorithm with a time step of 2 fs.[55] The cutoff values for electrostatic interactions and van der Waals interactions were both set to 1.2 nm. Long-range electrostatic interactions were computed using the particle mesh Ewald (PME) method.[56] The trajectories were analyzed using MDanalysis, MDtraj, and MD-IFP.[57−59] VMD was used for structure visualization.[60]

RESULTS

AL-Induced Transcriptomic Changes in *A. flavus*. We first tested the dry weight of mycelia and the glucose and NH_4^+ content in standard growth media (CK) and in media with AL added over the course of 6 days. This was to confirm the metabolic activity of mycelia in AL and CK media during growth and to choose the best growth stage at which to mycelia sample for the multiomics studies. As expected, glucose and NH_4^+ levels decreased faster in the AL media compared to the CK. These data suggested that AL promoted glucose and NH_4^+ consumption, especially in the first 3 days; this was consistent with the higher dry weight of mycelia (Figure 1A) and the increase in mycelia pellet number (Figure S1) in cultures grown with AL during this rapid growth stage. Images derived from scanning electron microscopy showed that mycelia pellet diameters were ∼2−3 mm in the CK media (Figure S2A), larger than the 0.8 mm pellets in the AL (Figure S2B). CK mycelia were covered by many adherents (Figure S2C,E), whereas AL mycelia had smooth surfaces (Figure S2D,F). Because we observed rapid mycelial growth from days 1 to 3 after inoculation and then slower growth from days 4 to 6 (Figure 1A), we chose mycelia sampled from days 1 to 3 (Figure 1B) for further experiments.

First, to identify DEGs in response to AL treatment, transcriptomic analysis was performed with RNA sequencing (RNA-seq) for CK- and AL-treated mycelia sampled after 1, 2, and 3 days of growth (Table S1). AL-treated mycelia sampled after 1 day (AL1) or 2 days (AL2) had fewer genes expressed than CK mycelia on the corresponding days (CK1 and CK2, respectively). However, the number of expressed genes was similar for AL-treated and CK mycelia sampled after 3 days (AL3 and CK3, respectively) (Figure S3A). There were more highly expressed genes in CK1 than in CK2 or CK3, whereas AL-treated mycelia showed the largest number of highly expressed genes on day 3 (Figure 1C; Tables S2 and S3). The most highly expressed genes were then analyzed based on two metrics: the fragments per kilobase of exon per million fragments mapped (FPKM) values, i.e., the highest overall normalized expression (Figure S3B) and $\log_2$(fold change) ($\log_2$ FC), i.e., those with the largest difference in expression between CK and AL-treated samples (Figure S3C). The density of the growth specificity index (gsi) for CK and AL peaked at 0.35 and 1, respectively, indicating that gene

https://doi.org/10.1021/acs.jafc.2c06230
J. Agric. Food Chem. XXXX, XXX, XXX−XXX

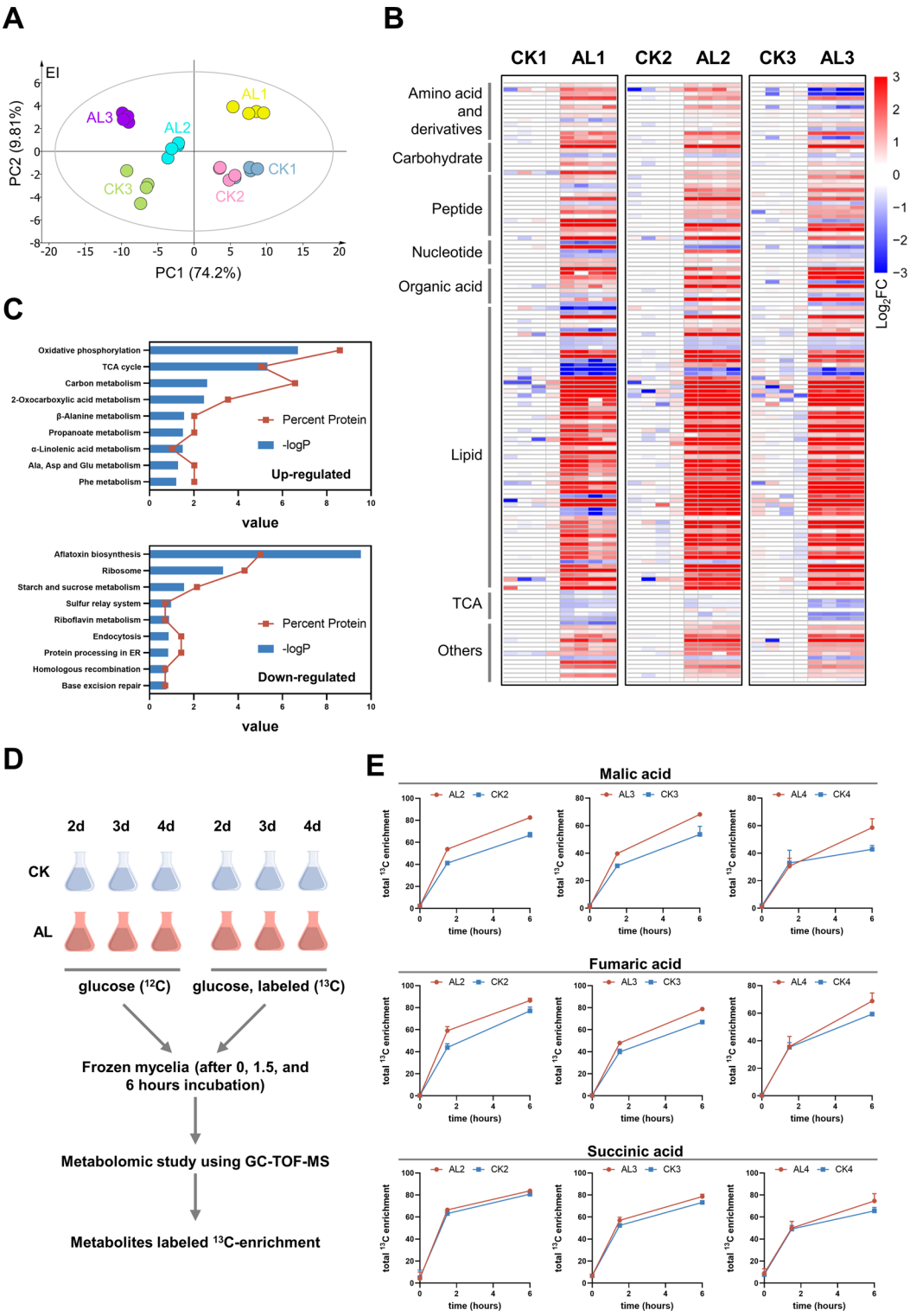

Figure 2. TCA cycle and oxidative phosphorylation were promoted by AL treatment. (A) PCA of the primary metabolome in mycelia samples detected by GC-MS demonstrates differences in the metabolomes of control mycelia (CK) and those treated with AL. (B) Heat map showing Log_2 FC values for 132 metabolites that were differentially accumulated between AL and CK mycelia samples over 3 days of growth. The relative abundance of each metabolite was normalized to the mean value from CK samples on different days. Metabolites were included in this analysis only if they were significantly differentially accumulated. Significant differences were observed at $p \leq 0.05$ (two-way analysis of variance (ANOVA)) with an additional false discovery rate (FDR) threshold of ≤0.05 to correct for multiple comparisons. (C) KEGG pathway enrichment analysis of upregulated and downregulated proteins. (D) Diagram of the experimental methods for ^{13}C labeling metabolic flux experiments. (E) Total ^{13}C enrichment of tricarboxylic acid cycle intermediates over time.

expression differences were more significant for AL than those for CK (Figure 1E).

There were 113 and 265 genes in CK- and AL-treated mycelia, respectively, that were consistently upregulated over

https://doi.org/10.1021/acs.jafc.2c06230
J. Agric. Food Chem. XXXX, XXX, XXX−XXX

days 1 through 3; CK- and AL-treated mycelia also showed 465 and 124 downregulated genes, respectively, over the same time. Additionally, there were many more upregulated genes in AL1 vs AL2 and AL2 vs AL3 than in CK1 vs CK2 and CK2 vs CK3, respectively, suggesting that the upregulated genes were more common in AL-treated mycelia during the 3-day incubation (Figure 1D and Table S4). In addition, we characterized nine patterns of gene expression from day 1 to day 3 (Figure 1F). In AL-treated mycelia, 22.92% of genes did not show significant changes during the 3-day incubation, compared to 49.90% in CK mycelia. This suggested that AL treatment caused regulation of more genes over time than CK, especially continuously upregulated genes (12.43 vs 3.16%) and genes upregulated only from day 2 to day 3 (20.91 vs 4.42%) (Figure 1F). Overall, the results showed remarkable differences in the number of expressed genes and the number of DEGs on the first 2 days of mycelial growth in CK or AL media, but these differences lessened by day 3. This was consistent with the observed morphological changes over time (Figures 1, S2, and S3).

DEGs were then analyzed for enrichment in KEGG biochemical pathway annotations. Significantly enriched pathways included amino acid metabolism, biosynthesis of secondary metabolites, carbohydrate metabolism, lipid metabolism, and so on (Figures 1G and S4; Tables S5−S7). Specifically, there were three amino acid metabolism pathways (tyrosine metabolism, phenylalanine metabolism, and arginine and proline metabolism); three carbohydrate metabolism pathways (glyoxylate and dicarboxylate metabolism, TCA cycle, and pentose and glucuronate interconversions); two energy metabolism pathways (methane metabolism and oxidative phosphorylation); and three lipid metabolism pathways (fatty acid biosynthesis, fatty acid degradation, and α-linolenic acid metabolism) upregulated by AL treatment (Figure S4). The AF biosynthesis pathway was classified as "biosynthesis of secondary metabolites" and other glycan degradation as "glycan biosynthesis and metabolism", and these were downregulated by AL treatment (Figure S4). Higher expression of proteins such as members of the GPI-anchored protein family, AFLA_068360 and AFLA_113120, in CK mycelia may help to form adhesions covering the outer surface, resulting in the observed large size and smooth, rounded surfaces (Figure S2C,E and Table S2).

AL Enhanced Primary Metabolism in *A. flavus*. To confirm AL-mediated regulation of these metabolic pathways in *A. flavus*, MS-based metabolomic and lipidomic analyses were performed using the same mycelia samples. GC-MS detected 56 peaks (Table S8); LC-MS detected 2451 and 3126 peaks in the positive and negative modes, respectively (Tables S9 and S10). In total, 500 primary and specialized metabolites were conclusively identified based on authentic standards. The mycelial lipidome was also investigated by LC-MS-based lipidomic analysis. A total of 511 and 61 peaks were detected in the positive and negative modes, respectively (Tables S11 and S12), and 123 lipid species were identified based on the MS/MS spectra and authentic standards. The principal component analysis (PCA) plots based on both metabolomic and lipidomic data showed separation between the AL-treated and the CK samples (Figures 2A and S5). The AL1, AL2, and AL3 samples were also clearly separated from one another, suggesting that larger metabolic differences existed in the AL-treated samples during growth compared with CK samples (Figure 2A). These results were consistent with the changes in gene expression observed in AL samples over time (Figure 1D).

There were 132 metabolites, including amino acids and derivatives, carbohydrates, peptides, nucleotides, organic acids, and lipids that were significantly differentially accumulated between AL and CK samples (Figure 2B). Most of the differentially accumulated primary metabolites were upregulated in AL samples. The levels of glucose and sucrose in AL-treated mycelia decreased over time, consistent with the faster glucose consumption from the liquid media (Figures 1A and S6A). The levels of most amino acids detected in this study changed significantly over time both for CK- and AL-treated mycelia (Figure S6B). Specifically, the levels of most amino acids that have been reported to support AF biosynthesis increased on days 1 and 2 but significantly decreased on day 3 (Figure S6B), consistent with the observed rapid NH_4^+ consumption from the liquid media (Figure 1A).

In addition, most differentially accumulated lipids were upregulated in AL-treated mycelia (Figure 2B). Specifically, lipid molecules containing C18:3 in the side chain, such as DG (18:3/18:2), PE (18:3/18:3), and PS (16:0/18:3), were significantly upregulated by AL treatment (Figure 2B). This was consistent with the transcriptome analysis, which showed that α-linolenic acid metabolism was upregulated by AL (Figure S4). However, several lipid molecules, such as DG (16:0p/18:1), DG (34:2e), DG (18:1p/18:1), PC (38:3), and PC (42:2), were downregulated by AL from day 1 to day 3. Notably, we also observed that levels of TCA cycle intermediates (e.g., succinic acid, fumaric acid, and malic acid) were decreased in AL samples (Figure 2B and Table S13), suggesting that AL treatment promoted TCA cycle activity to support faster mycelial growth. This hypothesis was in general agreement with the transcriptomic results.

To further confirm the effects of AL on the TCA cycle in *A. flavus*, proteomic analysis was performed in mycelia sampled on day 3 (CK3 and AL3). There were 2554 proteins identified in common between the CK3 and AL3 samples, 1531 of which were differentially expressed; these comprised 1032 upregulated and 499 downregulated proteins (Table S14). As expected, KEGG enrichment analysis of the differentially expressed proteins showed that the downregulated proteins were primarily enriched in the AF biosynthetic pathway (Figure 2C), whereas the upregulated proteins were significantly enriched in the TCA cycle and oxidative phosphorylation pathways (Figure 2C). qRT-PCR experiments confirmed that corresponding genes involved in the TCA cycle and oxidative phosphorylation were generally expressed at higher levels in AL-treated mycelia compared to CK samples (Figure S7). Integrated transcriptomic, metabolomic, and proteomic data thus revealed that AL treatment significantly promoted TCA cycle activity in *A. flavus*.

We also confirmed metabolic changes in TCA cycle intermediates during days one through three via ^{13}C-labeled metabolic flux analysis (^{13}C-MFA) (Figure 2D). At different time points, levels of ^{13}C-labeled malic acid, fumaric acid, and succinic acid were all higher in AL-treated mycelia than those in CK samples (Figure 2E). This suggested that the turnover rate of the TCA cycle was increased in AL-treated samples. Taken together, all of the data indicated that AL treatment promoted TCA cycle activity in *A. flavus*.

AL Activated the IMQ Biosynthetic Pathway in *A. flavus*. A previous study by our group demonstrated that AL inhibited AF biosynthesis but promoted kojic acid production

https://doi.org/10.1021/acs.jafc.2c06230
J. Agric. Food Chem. XXXX, XXX, XXX−XXX

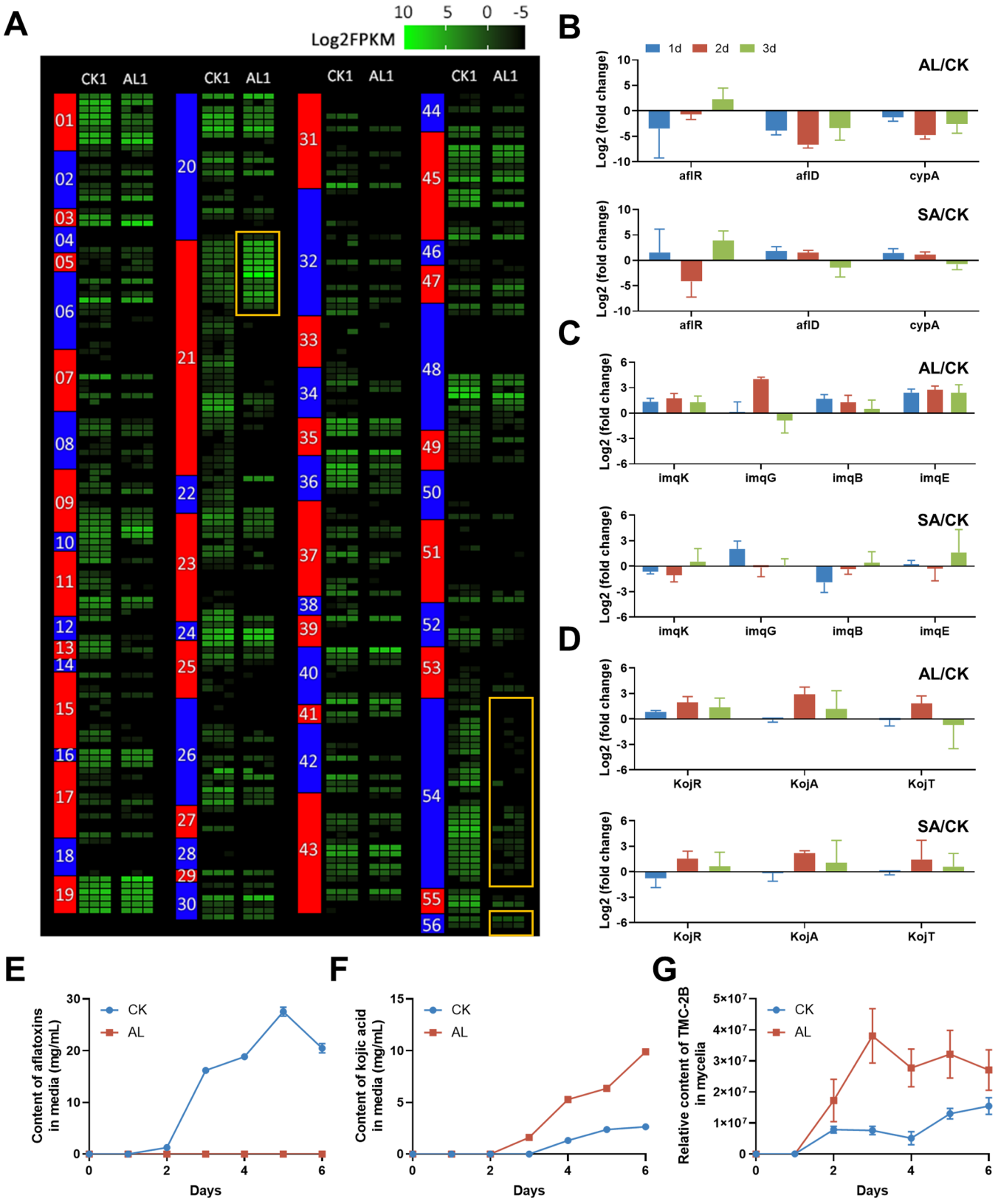

Figure 3. Impacts of AL treatment on specialized metabolite gene cluster expression. (A) Heat map showing expression of genes in specialized metabolite gene clusters in control (CK) and AL-treated mycelia after 1 day of growth. (B–D) Gene expression as measured via qRT-PCR. Expression changes are represented as the Log_2 FC of transcript abundance for genes encoding proteins involved in the biosynthesis of AF (B), imizoquins (C), or kojic acid (D) after AL or stearic acid (SA) treatment. Levels of AF (E) and kojic acid (F) over time. (G) Relative TMC-2B content in mycelia as measured by LC-MS.

https://doi.org/10.1021/acs.jafc.2c06230
J. Agric. Food Chem. XXXX, XXX, XXX−XXX

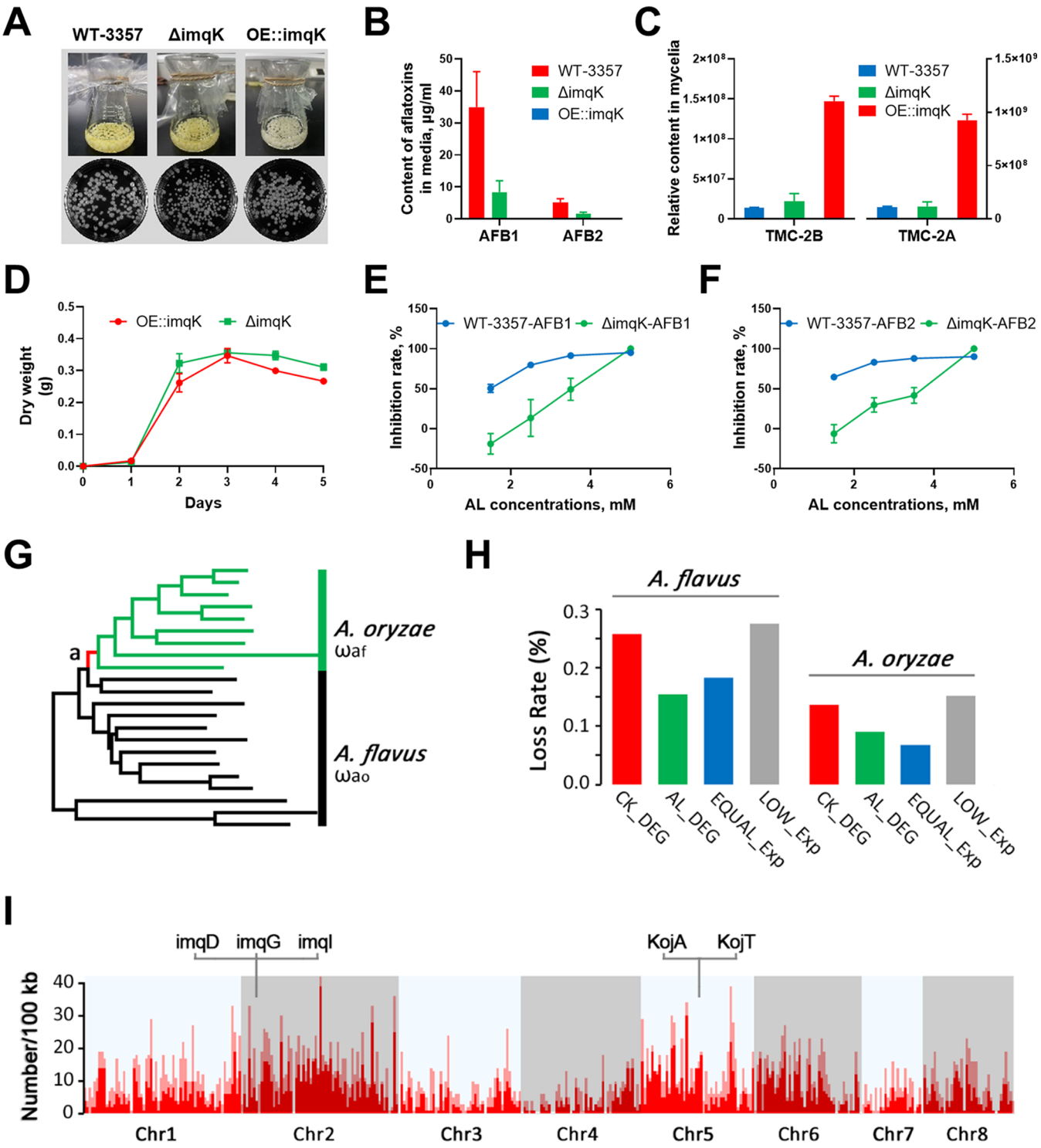

Figure 4. *imqK* overexpression or deletion affected aflatoxin (AF) production in *A. flavus* and genes involved in the IMQ gene cluster were positively selected in *A. oryzae*. (A) Mycelia phenotypes in WT-3357, ΔimqK, and OE::imqK strains after 3 days of incubation. (B) AF contents in the medium from the culture inoculated with the three strains. (C) Relative contents of TMC-2B and TMC-2A in the mycelia from the three strains. (D) Dry weight curve of ΔimqK and OE::imqK strains during 5 days of incubation. (E, F) Inhibition rate of AF production in WT-3357 or ΔimqK strains treated with different concentrations of AL. (G) Phylogenetic tree for further analysis of 13 *A. flavus* and nine *A. oryzae* strains. This maximum likelihood tree was constructed from 4927 orthologous protein-coding genes, and all nodes had >90% bootstrap support. "a" is the branch separating *A. oryzae* (foreground branch, green) and *A. flavus* (background branch, black) used in PAML CodeML. (H) Gene loss rate of DEGs in AL-treated samples (AL_DEG), in CK samples (CK_DEG), and genes that were stably expressed in the CK- and AL-treated samples (EQUAL_Exp) in *A. flavus* and *A. oryzae*. (I) Positively selected gene (PSG) density in *Aspergillus* chromosome. The *y*-axis indicates the copy number of positively selected genes per 100 kb detected by PAML CodeML.

in *A. flavus*.[19] This suggested that AL specifically regulates specialized metabolism *A. flavus*. In the present study, we measured the expression of genes in 56 specialized metabolite gene clusters based on the transcriptomic data. As expected,

https://doi.org/10.1021/acs.jafc.2c06230
J. Agric. Food Chem. XXXX, XXX, XXX−XXX

expression levels of most genes in the AF gene cluster (no. 54) were inhibited in AL-treated mycelia, and expression levels of most genes in the kojic acid gene cluster (no. 56) were increased, especially on day 3 (Figures 3A and S8D). In addition, we observed that expression levels of genes in 13 other specialized metabolite gene clusters were differentially regulated in response to AL treatment, with six significantly downregulated (Figure 3A). For example, expression levels of all genes in the cyclopiazonic acid gene cluster (no. 55) were significantly downregulated by AL, as were as most genes in the pigment gene cluster (no. 10) and the aspergillic acid gene cluster (no. 11). Genes in two unknown gene clusters (nos. 12 and 13) were also inhibited by AL. Surprisingly, AL treatment significantly promoted the expression of genes in the IMQ gene cluster, a recessive biosynthetic gene cluster in the upper part of gene cluster no. 21[23] (Figure 3A). More importantly, the high expression levels of genes in the IMQ cluster were maintained over time (Figure S8B), whereas genes in the kojic acid cluster were downregulated by AL treatment on day 1 and then gradually upregulated from day 2 to day 3 (Figure S8D). This suggested that the IMQ gene cluster was the only specialized metabolite gene cluster continuously upregulated by AL.

To further confirm the effects of AL on specialized metabolite pathways in *A. flavus*, qRT-PCR experiments and targeted metabolite analysis were performed. The qRT-PCR results showed that genes in the AF gene cluster were downregulated by AL treatment, whereas genes in the IMQ and kojic acid gene clusters were upregulated (Figure 3B−D, up rows). These results were consistent with the RNA-seq data. Furthermore, targeted metabolite quantification showed that AL treatment inhibited AF production and promoted kojic acid production in *A. flavus* (Figure 3E,F). More importantly, relative levels of TMC-2B and TMC-2A, which are the metabolic intermediates of the IMQ pathway, were significantly increased in AL-treated mycelia from day 2 (Figures 3G and S9), indicating that AL activated the IMQ pathway and promoted IMQ biosynthesis in *A. flavus*.

Because our previous study showed that SA promoted AF biosynthesis in *A. flavus*,[19] we further measured the expression of genes in the IMQ gene cluster after treatment with SA. SA treatment suppressed the expression of several genes in the IMQ gene cluster on days 1 and 2 (Figure 3C) but promoted the expression of genes in the kojic acid gene cluster (Figure 3D). Taken together, these results suggest that AL inhibited AF production and specifically activated the IMQ biosynthetic pathway in *A. flavus*.

IMQ Biosynthesis Was Negatively Correlated with AF Production. To further investigate the relationship between the IMQ gene cluster and AF production, we observed the results of overexpressing or deleting a transcription factor gene in the IMQ gene cluster, *imqK*, in *A. flavus* (strains OE::imqK and ΔimqK, respectively). Mycelia pellets of both the OE::imqK and ΔimqK strains were similar in size to those of the wild-type NRRL 3357 strain (WT-3357), and there was no significant difference between the growth rate of OE::imqK and ΔimqK (Figure 4A,D). However, AF production was decreased in the ΔimqK strain and completely inhibited in the OE::imqK strain compared with the WT-3357 (Figure 4B). A previous study revealed that genes in the IMQ cluster were expressed at significantly higher levels in the OE::imqK strain and that IMQ production was promoted.[23] Consistent with those results, levels of TMC-2B and TMC-2A were much higher in the OE::imqK strain than in the WT-3357 or the ΔimqK strain using targeted metabolite analysis (Figure 4C). These results suggested that IMQ biosynthesis was negatively correlated with AF production in mycelia. We, therefore, treated ΔimqK and WT-3357 using AL with a range of concentrations to examine the effects of preventing the IMQ pathway on AF production. As expected, although AL treatment still inhibited AF biosynthesis in the ΔimqK strain, the inhibition rate was much lower than in the WT-3357 (Figure 4E,F). Taken together, these results indicated that IMQ may be a key factor in the observed AL-mediated AF biosynthesis inhibition.

To further understand the relationship between the IMQ gene cluster and AF production, we tested whether the IMQ gene cluster was positively selected in *A. oryzae*, a closely related species of *A. flavus* that does not produce AF.[61] First, we compared the genomes of 22 assembled *A. flavus* and *A. oryzae* strains downloaded from NCBI and AspGD[39] (Table S15). The 1:1 orthologs were built and the gene loss rate was calculated between the 13 *A. flavus* and nine *A. oryzae* strains (Figure 4G). All *A. flavus* protein-coding genes were divided into four classes: (1) genes only expressed in CK samples (CK_DEG); (2) genes only expressed in AL-treated samples (AL_DEG); (3) genes that were stably expressed between CK and AL-treated *A. flavus* samples (EQUAL_Exp); and (4) lowly expressed genes (LOW_Exp). Of the four classes of genes, the gene loss rate was much higher in CK_DEG (25.72%) than that in AL_DEG (15.38%) in the 13 *A. flavus* strains (Figure 4H). This indicated that CK_DEG genes may play regulatory roles in different environments. In the nine *A. oryzae* strains, gene loss was also much higher in CK_DEG (13.64%) than that in AL_DEG (8.97%) or EQUAL_Exp (6.79%). Gene loss was lower in AL_DEG than that in EQUAL_Exp in *A. flavus*, whereas the rate of loss was higher in AL_DEG than that in EQUAL_Exp in *A. oryzae* (Figure 4H). Because AF production does not occur in *A. oryzae*, these results indicate that most genes in the AL_DEG class in *A. flavus* play major roles in promoting mycelial growth, which allows strains of that species to survive via rapid growth.

Positive selection during evolution was then examined using branch-site models. These analyses yielded 1899 nonredundant positively selected genes (PSGs) at FDR <0.05 and 1282 PSGs at FDR <0.005 in *A. oryzae*-specific branches (Table S16). Using the 1282 sites detected as positively selected at FDR <0.005, we plotted the positive selection distribution of each chromosome in the *A. oryzae* genome (Figure 4I). The results showed that *imqD*, a member of the IMQ gene cluster, was classified as positively selected at FDR <0.005; two other genes in this cluster, *imqG* and *imqI*, were classified as positively selected at FDR <0.05 (Table S16). Furthermore, the kojic acid gene cluster members *kojA* and *kojT* were also positively selected at FDR <0.05, and no selection was detected for genes in the AF gene cluster (Table S16). These results indicated that, in addition to the loss of the AF gene cluster, the evolution of *A. oryzae* from *A. flavus* may have involved key roles for genes in the IMQ and kojic acid gene clusters.[61,62] Taken together, these results demonstrated that AL specifically activated the IMQ gene cluster in *A. flavus* and that several genes in this cluster were positively selected during the evolution of the non-aflatoxigenic strain *A. oryzae*.

ImqJ as a Potential AL-Interacting Receptor Protein. To identify the potential receptor protein that perceived and interacted with exogenous AL, we performed thermal

https://doi.org/10.1021/acs.jafc.2c06230
J. Agric. Food Chem. XXXX, XXX, XXX−XXX

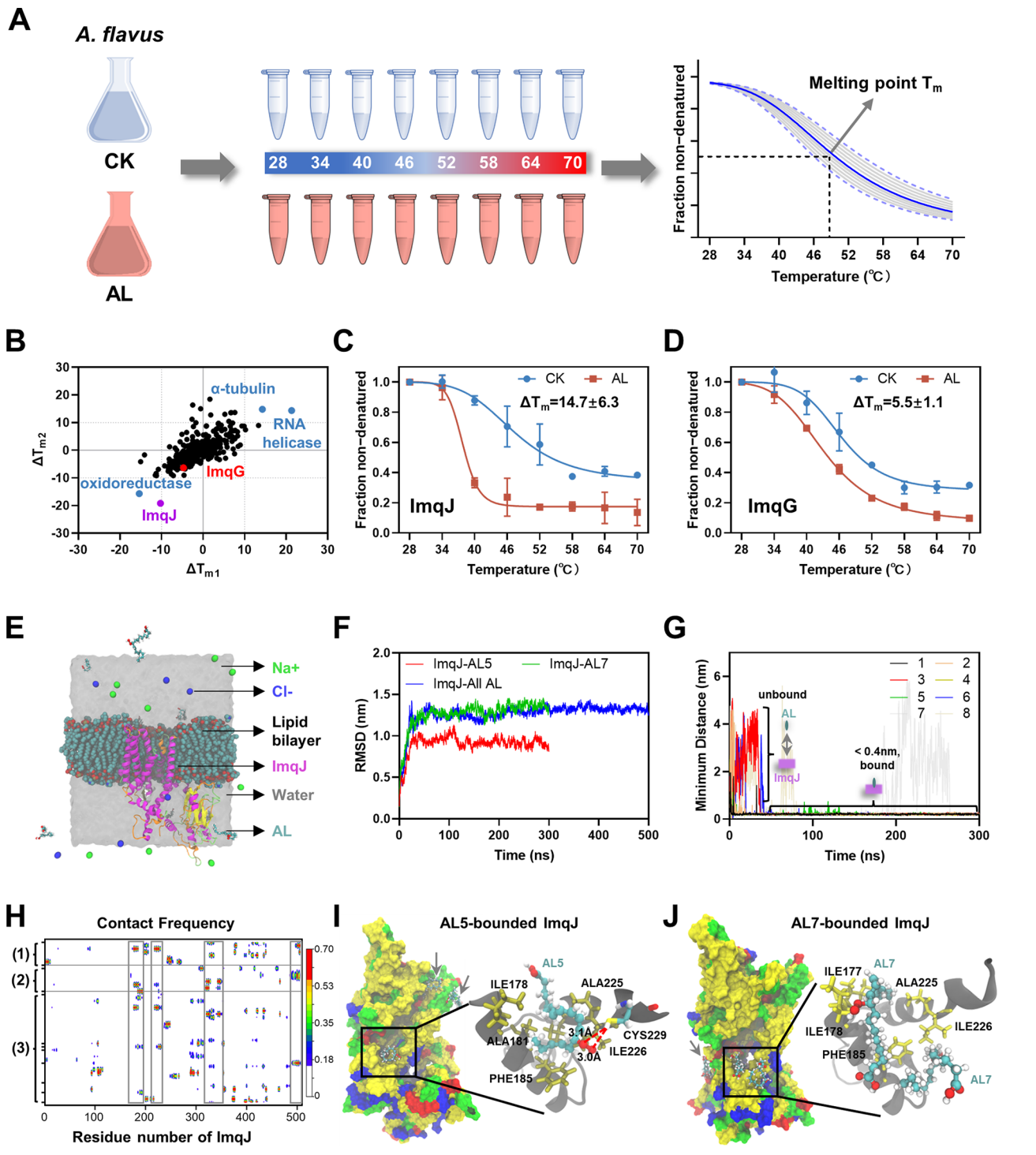

Figure 5. Characterization of interactions between AL and ImqJ. (A) Experimental design of thermal proteome profiling experiments. Protein samples were incubated at temperatures from 28 to 70 °C. Soluble proteins were analyzed from each fraction using quantitative mass spectrometry. Proteins for which we obtained high-quality melting curves, i.e., fitted R^2 values 0.95, were used in further analyses. (B) Comparison of protein T_m shifts determined from two biological replicates. Melting curves for ImqJ (C) and ImqG (D), which are involved in IMQ biosynthesis. Error rates were calculated from two independent replicate experiments. (E) Diagram showing a molecular dynamics simulation system. ImqJ was embedded in a lipid bilayer in the presence of AL molecules. (F) Root mean square deviation (RMSD) plots for the protein backbone in the three simulations. ImqJ-AL5, ImqJ-AL7, and ImqJ-All AL represent the systems containing ~6 mM 13-HPOTE (AL5), 6 mM 9-HPOTE (AL7), and a 25 mM mixture of AL molecules. (G) Plots showing variation in the minimum distance between AL7 molecules and ImqJ over time. When the minimum distance changed at the nanometer scale, AL did not bind to ImqJ. After AL bound to ImqJ, the minimum distance was typically smaller than 0.4 nm. (H) Contact map for ImqJ and AL molecules obtained from the simulation trajectories. 1, 2, and 3 represent the maps for ImqJ-AL5, ImqJ-AL7, and ImqJ-All AL, respectively. Structural representation of ImqJ-AL5 and ImqJ-AL7, showing one AL5 (I) and two AL7 (J) molecules bound to the ImqJ hydrophobic pocket, which consisted of two α-helices (residues 177−191 and 215−229). AL molecules that bound to other ImqJ residues are indicated with gray arrows.

https://doi.org/10.1021/acs.jafc.2c06230
J. Agric. Food Chem. XXXX, XXX, XXX−XXX

Table 1. Proteins Significantly Affected by AL Treatment

protein ID	protein name	ΔT_{m1}	ΔT_{m2}	R^2 of fitting			
				control 1	control 2	treatment 1	treatment 2
AFLA_080920	α-tubulin	14.27	14.84	0.986	0.9823	0.967	0.953
AFLA_112180	RNA helicase	21.33	14.37	0.998	0.999	0.968	0.958
AFLA_064320	peptide transporter imqJ	−10.24	−19.20	0.992	0.956	0.993	0.983
AFLA_124330	short-chain oxidoreductase/dehydrogenase	−15.34	−15.65	0.991	0.961	0.986	0.989

proteome profiling (TPP) assays in CK- and AL-treated *A. flavus* samples after 1 day of growth. This enabled us to monitor changes in thermal stability across the mycelial proteome using quantitative MS. Using this technique, a protein with an altered melting point (T_m) is considered a receptor for the compound being tested.[36] Protein extracts of both CK- and AL-treated mycelia were treated at eight different temperatures ranging from 28 to 70 °C (Figure 5A). There were 2214 and 2472 proteins quantified in the CK- and AL-treated samples, respectively (Table S17). Four proteins, namely, α-tubulin, RNA helicase, the peptide transporter ImqJ, and short-chain oxidoreductase/dehydrogenase, showed significant T_m shifts in response to AL treatment (Figure 5B and Table 1). The melting points of α-tubulin and RNA helicase increased, indicating stabilization by AL, whereas those of ImqJ and short-chain oxidoreductase/dehydrogenase decreased, indicating AL-induced destabilization (Figure 5B,C). Interestingly, AL destabilized the transporter ImqJ, which is involved in IMQ biosynthesis, revealing ImqJ as a potential receptor of AL. The average T_m of ImqJ was 53.5 °C in CK samples and 38.8 °C in AL-treated samples. ImqG, which is also located in the *imq* gene cluster, did not show significant changes (Figure 5C,D). These results suggested that not only did AL promote the expression of genes in the IMQ gene cluster, but that the transporter protein ImqJ was involved in AL signal transduction.

ImqJ Interacted with AL through Hydrophobic Interactions. To gain insights into the interactions between ImqJ and AL, we used ColabFold, a protein structure prediction server powered by the highly accurate artificial intelligence (AI) structural prediction program AlphaFold2 to predict the structure of ImqJ.[45,46] The amino acid sequence of ImqJ was submitted to the ColabFold server and five structural models were predicted by AlphaFold2. The predicted local-distance difference test (pLDDT) showed that the major part of each structure was predicted with high confidence (pIDDT > 90, Figure S10). Thus, the model with the highest average pIDDT value was used as the starting structure in all-atom MD simulations to investigate the interaction between ImqJ and AL.[63] The primary aim of these MD simulations was to determine whether an interaction between AL and ImqJ could be observed. The simulation systems included an ImqJ protein inserted into a lipid bilayer, ions, water, and AL molecules (Figure 5E).

Our previous study showed that AL contains different proportions of eight oxylipin species: 9,14-diHPOTE; 9,15-diHPOTE; 9,16-diHPOTE; 13,16-diHPOTE; 9,11-diHPOTE; 9-HPOTE; 13-HPOTE; and 17-HPOTE (AL1−AL8, respectively).[19] To study the interaction between AL and ImqJ, three different systems were investigated, namely, one with AL7 (ImqJ-AL7), one with AL5 (ImqJ-AL5), and one with a mixture of the eight oxylipin species (ImqJ-ALL AL); additional details about these systems can be found in the Materials and Methods. AL molecules were initially placed far from ImqJ without noncovalent interactions. The simulations with ImqJ-AL7, ImqJ-AL5, and ImqJ-All AL were performed for a duration of 300, 300, and 500 ns, respectively, for a total simulation time of 1.1 μs. The stability and equilibration of the MD simulations were examined by measuring the root mean square deviation (RMSD) fluctuations of the proteins, which showed that all simulation systems equilibrated after ∼25 ns (Figure 5F). The minimum distance between ImqJ and AL7 over the simulation time in the ImqJ-AL7 system was calculated to illustrate the possible binding of AL to ImqJ. The distance initially fluctuated on a scale of a few nanometers, which was reasonable because the AL molecules had been placed far from ImqJ to start and could freely diffuse in the solution (Figure 5G). Several AL7 molecules collided with the possible binding sites on ImqJ after ∼50 ns. This led to a minimum stable distance of <4 Å, a distance consistent with noncovalent interactions.

To further investigate the interactions between AL molecules and ImqJ in all simulation systems, we performed a contact map analysis using MDTraj.[58] This analysis was used to monitor the contacts between AL and ImqJ and to calculate the contact frequency during each simulation. Some residues of ImqJ frequently contacted AL molecules, with a rate >0.5 in all simulation systems (Figure 5H), suggesting that these ImqJ residues interacted with AL. An interaction fingerprint (IFP) analysis was then performed to identify the specific interactions between AL and ImqJ.[64] Between the two types of analyses, we observed the binding of 32 ImqJ residues to AL (contact frequency >0.5) (Table S18). Almost all of these residues interacted with AL via hydrophobic interactions; some residues also bound to AL through water bridges or hydrogen bonds. Specifically, a hydrophobic binding pocket consisting of two α-helices (residues 177−191 and 215−229) was observed in ImqJ in all three systems (Figure 5H−J). In the center structure of the ImqJ-AL5 system, one AL5 molecule bound to residues ILE178, ALA181, PHE185, ALA225, and ILE226 through hydrophobic interactions, and its two peroxide-forming oxygen atoms formed hydrogen bonds with CYS229 (Figure 5I). In the center structure of the ImqJ-AL7 system, two AL7 molecules bound to the hydrophobic pocket, primarily through interactions of residues similar to those observed in the simulation with AL5 (Figure 5J). Taken together, the MD simulation results suggested that ImqJ could bind to AL primarily through hydrophobic interactions.

Proposed Model of AL-Mediated AF Inhibition. We next sought to understand the possible relationships between genes involved in AL-mediated regulation of AF biosynthesis and cell signaling pathways based on our results and knowledge of the genes involved in regulation of AF biosynthesis in *A. flavus* as summarized by Caceres et al. (Table S19).[3] We therefore selected 188 genes and constructed an interaction regulatory network using STRING v11.0.[65] Genes without interactions found in the database were discarded, resulting in a final network containing 150 genes

https://doi.org/10.1021/acs.jafc.2c06230
J. Agric. Food Chem. XXXX, XXX, XXX−XXX

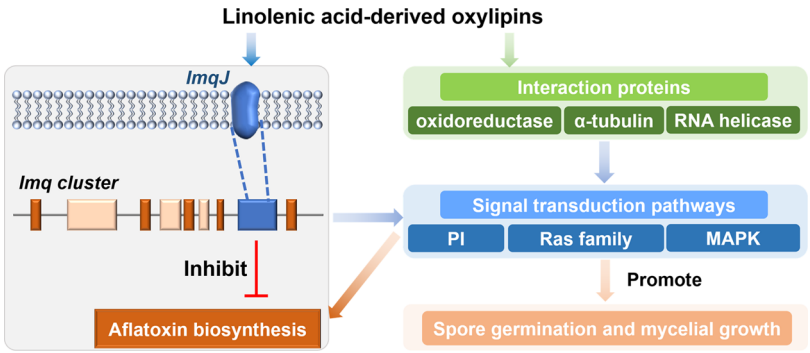

Figure 6. Proposed model of AL-mediated AF inhibition and mycelial growth in *A. flavus*.

(Figure S11). Our transcriptome data showed that most reported regulatory proteins were downregulated in AL-treated samples on day 1 and then gradually reached expression levels comparable to those in the CK samples on day 3 (Figures S11−S13). These included genes in the IMQ gene cluster, RasA, and FadA; in contrast, genes in the phosphatidylinositol (PI) and mitogen-activated protein kinase (MAPK) pathways were upregulated from day 1 (Figure S11). The IMQ gene cluster was connected to PI and MAPK pathways through an anthranilate synthase multifunctional protein, TrpC. In addition, the putative nonribosomal peptide synthase ImqB and putative transcription factor ImqK were linked to AflC and AflF, respectively, which are members of the AF biosynthesis gene cluster. However, no interaction partner of ImqJ was identified in this database.

qRT-PCR experiments were performed to verify the expression of genes in the network (Figure S14). The results showed that GPCRs were downregulated on day 1 and that some GPCR genes were more highly expressed in AL-treated samples than those in CK samples on days 2 and 3 (Figure S15A). Genes involved in the PI and MAPK pathways were predominantly upregulated (Figure S15A). These results were in general agreement with the transcriptome data. Moreover, our metabolome data showed that levels of PIs containing fatty acid 18:3, except for PI (18:1/18:3), were higher in AL-treated samples (Figure S15B). In contrast, levels of other fatty acids were generally lower in AL-treated than those in CK samples, suggesting that PI biosynthesis was regulated by AL (Figure S15B). It has been shown in recent studies that PI signaling is involved in regulation of the MAPK pathway and controls filamentous fungal growth.[66,67] Additionally, oxidative stress is considered to be an important factor in AF synthesis.[3] Superoxide dismutase (SOD), catalase (CAT), and glutathione peroxidase (GPX) are key enzymes in fungal protection against reactive oxygen species (ROS).[68] The genes encoding these enzymes were expressed at lower levels in AL-treated samples than those in CK samples on day 1 but were expressed at higher levels in AL-treated samples compared to CK samples on day 3 (Figure S16). Highly oxygenated molecules are a prerequisite for AF biosynthesis. High levels of ROS-inactivating substances and antioxidants, such as IMQs and kojic acid, can inhibit AF production by reducing oxidative stress levels.

In summary, we propose a model based on the results of this study (Figure 6). AL binds to ImqJ and enhances IMQ biosynthesis, which inhibits AF production. AL also binds to other protein receptors, regulating signal transduction pathways and affecting germination and mycelial growth. Based on the protein interaction network, proteins involved in IMQ biosynthesis could also interact with signaling-related proteins, which would then affect AF biosynthesis; ultimately, this would almost completely inhibit AF synthesis, promoting mycelial germination and growth.

DISCUSSION

AF, which is produced by *A. flavus*, can pollute many types of crops, causing great economic losses. A series of studies have identified numerous compounds that can regulate and inhibit AF biosynthesis.[9−12,19,69−71] However, AF production is a very complicated process that is regulated by various signaling pathways, making the mechanism(s) of regulation difficult to understand. Our previous work showed that stearic acid and linolenic acid promote AF production, whereas AL inhibits it.[19] The mechanisms by which AL inhibits AF biosynthesis are unclear. In the present study, we combined comprehensive omics analyses, MD simulations, and functional validation experiments to examine the role of AL in regulating AF biosynthesis. *A. flavus* supplied with AL showed overall changes in phenotypes and gene expression; in particular, the dry weight and number of mycelia increased, and the TCA cycle, oxidative phosphorylation, and amino acid metabolism were promoted. Although AF production was inhibited by AL treatment, biosynthesis of IMQs, a newly discovered class of fungal isoquinoline alkaloids, was specifically promoted. TPP assays and MD simulations showed that the transporter protein ImqJ could bind to AL. Furthermore, AF biosynthesis was barely detectable when the transcription factor ImqK, a member of the IMQ gene cluster, was overexpressed; deletion of ImqK weakened the inhibitory effect of AL. Overall, the results revealed that the *A. flavus* IMQ biosynthetic pathway played a key role in inhibiting AF production, demonstrating a novel direction for development of strategies to prevent AF contamination in crops.

TCA Cycle Was Involved in the *A. flavus* Response to AL. The TCA cycle has previously been shown to play important roles in regulating AF biosynthesis. Acetate is the primary molecule in both the AF biosynthesis pathway and the TCA cycle, suggesting a relationship between the two processes.[72] Fountain et al. examined the proteomes of select isolates of *A. flavus* in response to increasing levels of H_2O_2-derived oxidative stress, which has been shown to be a prerequisite for and stimulator of AF production. The results demonstrated that the TCA cycle, glycolysis, oxidative phosphorylation, amino acid catabolism, and complex macromolecular catabolism comprise the bulk of pathways that are differentially regulated in response to H_2O_2 treatment.[73]

https://doi.org/10.1021/acs.jafc.2c06230
J. Agric. Food Chem. XXXX, XXX, XXX−XXX

Analysis of the coregulatory gene expression network under conditions with and without AF production occurring showed that the expression levels of genes involved in the TCA cycle and glycolysis were significantly reduced in the non-aflatoxigenic conditions.[74] Pan et al. showed that dimethylformamide inhibition of AFB1 biosynthesis may be due to downregulation of pathways related to the TCA cycle and glycolysis.[75] Here, our multiomics, qRT-PCR, and ^{13}C-glucose parallel labeling results together revealed that AL promoted the TCA cycle. This demonstrated that the TCA cycle is involved in the response to AL and regulation of AF biosynthesis. Together with previous studies, these results suggest that the role of the TCA cycle in regulating AF biosynthesis could vary under different conditions.

IMQ Gene Cluster Plays Versatile Roles in the *A. flavus* Response to AL. Previous genome analysis predicted the existence of at least 56 specialized metabolite gene clusters in *A. flavus*.[76] Of the 56 specialized metabolic pathways, our transcriptomic, metabolomic, and qRT-PCR experiments consistently showed that the kojic acid biosynthesis pathway was upregulated on days 2 and 3 and that the IMQ biosynthesis pathway was significantly upregulated from day 1. Expression levels of the AF, IMQ, and kojic acid gene clusters in response to SA and AL treatment suggested that the IMQ gene cluster was specifically up-regulated by AL. Previous studies showed that the ralstonins (lipopeptides produced by the plant pathogenic bacterium *Ralstonia solanacearum*) downregulated expression of genes in the IMQ gene cluster; the same study also suggested that IMQs, which resist oxidative stress, are necessary for normal germination of *A. flavus*, and that overexpression of the transcription factor *imqK* accelerated *A. flavus* germination.[23] Moreover, a recent study found that the expression levels of IMQs in *A. flavus* grown under antagonistic biological stress were higher.[77] These observations indicated that IMQ synthesis may play a role in the growth of AL-treated mycelia. Consistent with these observations, we found that AL treatment increased the number of mycelia pellets (Figure 1B). Furthermore, it has been proposed that AF biosynthesis in *A. flavus* is a component of the fungal oxidative stress response.[3,78−80] These findings suggest that IMQs, as antioxidants, could be key factors in regulating the AF biosynthesis gene cluster by resisting oxidative stress.

Our results also showed AL binding to the transporter ImqJ, changes in AF production in ImqK overexpression and deletion strains (OE::imqK and ΔimqK, respectively), and lower inhibition of AF production in response to AL treatment in the ΔimqK strain. Together, these results revealed a significant role of the IMQ biosynthesis pathway in regulating AF production. Consistent with our observations, four of the 11 genes in the IMQ cluster were found to be upregulated in non-aflatoxigenic isolates of *A. flavus*.[81] Interestingly, our analysis showed that some genes in this cluster were positively selected in *A. oryzae*, which does not produce AFs; this suggests that the IMQ and AF gene clusters have different functions in fungal evolution. Some interactions were found between the IMQ/AF gene clusters and signaling pathways in the STRING database. However, the details of how the IMQ gene cluster inhibits AF biosynthesis, whether by modulating the level of oxidative stress required or by other mechanisms, remain unclear and require further characterization in the future.

Kojic Acid May Indirectly Inhibit AF Biosynthesis by Reducing Oxidative Stress. Significant differential expression was observed in genes involved in kojic acid biosynthesis from day 2 to day 3. Previous studies have shown the tolerance of kojic acid biosynthesis to oxidative stress, demonstrating that kojic acid is an effective antioxidant.[82,83] Kojic acid production has been proposed to alleviate the increased oxidative stress caused by the loss of *msnA*, a putative stress regulatory gene.[82] In addition, our previous study showed that D-glucal effectively inhibited AF biosynthesis and promoted kojic acid biosynthesis in *A. flavus*.[84] In fact, a negative correlation between kojic acid and AF production has been proposed.[82−85] More importantly, a recent study showed that, under stress conditions, genes involved in AF biosynthesis were downregulated, whereas several genes involved in kojic acid and IMQ biosynthesis were upregulated,[85] consistent with our observations. These findings together suggest that the inhibition of AF biosynthesis may occur indirectly through reduced oxidative stresses from kojic acid biosynthesis.

It has been proposed that fungal cells regulate the activation of genes in specialized metabolic pathways and the flow of primary metabolites via a complex molecular switch mechanism, responding to possible environmental stressors through these molecular switches to enhance fungal cell survival.[86] Our results showed that, in response to AL treatment, *A. flavus* promoted growth by simultaneously regulating primary metabolism (e.g., the TCA cycle and oxidative phosphorylation) and specialized metabolism (e.g., IMQs, kojic acid, and AF biosynthesis), consistent with the molecular switch mechanism.

In summary, we utilized a multidisciplinary approach to explore the underlying mechanism of AL-mediated AF biosynthesis regulation in *A. flavus*. We found that the IMQ gene cluster plays a key role in inhibiting AF production. Further exploration of the molecular mechanism by which the IMQ gene cluster inhibits AF biosynthesis is of great significance in formulating effective AF prevention and control strategies.

■ ASSOCIATED CONTENT

Supporting Information

The Supporting Information is available free of charge at https://pubs.acs.org/doi/10.1021/acs.jafc.2c06230.

Additional description of materials and methods; photos of mycelium pellet of *A. flavus* that grown in the GMS liquid media (Figure S1); scanning electron microscopy images (Figure S2); RNA-seq-based transcriptomic data of CK and AL samples (Figure S3); KEGG enrichment of differentially expressed genes (Figure S4); PCA plots of metabolome in mycelia samples (Figure S5); relative abundance of sugars and amino acids (Figure S6); expression levels of genes involved in the TCA cycle and oxidative phosphorylation (Figure S7); $\log_2$ FC of FPKM values of genes involved in the secondary metabolic pathways (Figure S8); TMC-2A content in mycelia (Figure S9); structure prediction of ImqJ (Figure S10); protein−protein interaction networks and diagram (Figures S11−S14); validation of gene expression in the interaction network (Figure S15); $\log_2$ FC of FPKM value of genes involved in the signal transduction pathway (Figure S16) (PDF)

https://doi.org/10.1021/acs.jafc.2c06230
J. Agric. Food Chem. XXXX, XXX, XXX−XXX

Processed format of the transcriptomics, metabolomics, lipidomics, and proteomics data sets (Tables S1−S14), assembly for evolutionary genomic analysis (Table S15), positively selected genes (Table S16), output results of TPP experiments (Table S17), list of ImqJ residues that interact with AL (Table S18), and list of genes used to build the interaction network (Table S19) (XLSX)

AUTHOR INFORMATION

Corresponding Author

Shijuan Yan − *Guangdong Key Laboratory for Crop Germplasm Resources Preservation and Utilization, Agro-biological Gene Research Center, Guangdong Academy of Agricultural Sciences, Guangzhou 510640, China;* orcid.org/0000-0002-6907-1179; Email: shijuan@agrogene.ac.cn

Authors

Shaowen Wu − *Guangdong Key Laboratory for Crop Germplasm Resources Preservation and Utilization, Agro-biological Gene Research Center, Guangdong Academy of Agricultural Sciences, Guangzhou 510640, China*

Qunjie Zhang − *Guangdong Key Laboratory for Crop Germplasm Resources Preservation and Utilization, Agro-biological Gene Research Center, Guangdong Academy of Agricultural Sciences, Guangzhou 510640, China; Institution of Genomics and Bioinformatics, South China Agricultural University, Guangzhou 510642, China*

Wenyang Zhang − *Guangdong Key Laboratory for Crop Germplasm Resources Preservation and Utilization, Agro-biological Gene Research Center, Guangdong Academy of Agricultural Sciences, Guangzhou 510640, China*

Wenjie Huang − *Guangdong Key Laboratory for Crop Germplasm Resources Preservation and Utilization, Agro-biological Gene Research Center, Guangdong Academy of Agricultural Sciences, Guangzhou 510640, China*

Qian Kong − *Guangdong Key Laboratory for Crop Germplasm Resources Preservation and Utilization, Agro-biological Gene Research Center, Guangdong Academy of Agricultural Sciences, Guangzhou 510640, China*

Qinjian Liu − *Guangdong Key Laboratory for Crop Germplasm Resources Preservation and Utilization, Agro-biological Gene Research Center, Guangdong Academy of Agricultural Sciences, Guangzhou 510640, China*

Wenyan Li − *Guangdong Key Laboratory for Crop Germplasm Resources Preservation and Utilization, Agro-biological Gene Research Center, Guangdong Academy of Agricultural Sciences, Guangzhou 510640, China*

Xinlu Zou − *Guangdong Key Laboratory for Crop Germplasm Resources Preservation and Utilization, Agro-biological Gene Research Center, Guangdong Academy of Agricultural Sciences, Guangzhou 510640, China*

Chun-Ming Liu − *Key Laboratory of Plant Molecular Physiology, Institute of Botany, Chinese Academy of Sciences, Beijing 100093, China*

Complete contact information is available at: https://pubs.acs.org/10.1021/acs.jafc.2c06230

Author Contributions

S.Y. conceived and designed the project. Q.K., W.H., X.Z., Q.L., and S.W. performed the biochemical experiments. Q.Z. performed the transcriptome and bioinformatics analysis. W.Z., W.L., Q.K., and S.Y. performed proteomic analysis. W.H., S.W., and Q.K. performed the metabolomic and lipidomic analyses. W.Z. and S.W. performed thermal proteome profiling experiments. S.W. performed molecular dynamics simulations. S.Y., S.W., and Q.Z. wrote the manuscript. All authors contributed to data interpretation.

Funding

The authors gratefully acknowledge the support by the Natural Science Foundation of China (no. 31500045), the Special Fund for Scientific Innovation Strategy-Construction of High Level Academy of Agriculture Science (R2021YJ-YB1004 and R2020PY-JX019), the Natural Science Foundation of Guangdong Province (2014A030310489), and the Guangdong Special Support 318 Program (to Q.Z. and to S.Y., no. 2021TQ06N115).

Notes

The authors declare no competing financial interest.

‖S.W., Q.Z., and W.Z. are co-first authors.

ACKNOWLEDGMENTS

The authors thank Prof. Nancy P. Keller from the University of Wisconsin—Madison for providing the ΔimqK and OE::imqK strains, Dr. Saleh Alseekh, and Prof. Alisdair R. Fernie from Max Planck Institute of Molecular Plant Physiology for suggestions about the ^{13}C labeling metabolic flux experiments and Dr. Qingshi Meng from Chinese Academy of Agricultural Sciences for suggestions about the thermal proteome profiling assay.

REFERENCES

(1) Amaike, S.; Keller, N. P. *Aspergillus flavus*. *Annu. Rev. Phytopathol.* **2011**, *49*, 107−133.

(2) Yu, J.; Cleveland, T. E.; Nierman, W. C.; Bennett, J. W. *Aspergillus flavus* genomics: gateway to human and animal health, food safety, and crop resistance to diseases. *Rev. Iberoam. Micol.* **2005**, *22*, 194−202.

(3) Caceres, I.; Khoury, A. A.; Khoury, R. E.; Lorber, S.; Oswald, I. P.; Khoury, A. E.; Atoui, A.; Puel, O.; Bailly, J. D. Aflatoxin Biosynthesis and Genetic Regulation: A Review. *Toxins* **2020**, *12*, No. 150.

(4) Liao, J.; He, Z.; Xia, Y.; Lei, Y.; Liao, B. A review on biosynthesis and genetic regulation of aflatoxin production by major *Aspergillus* fungi. *Oil Crop Sci.* **2020**, *5*, 166−173.

(5) Chang, P. K.; Scharfenstein, L. L.; Ehrlich, K. C.; Wei, Q.; Bhatnagar, D.; Ingber, B. F. Effects of *laeA* deletion on *Aspergillus flavus* conidial development and hydrophobicity may contribute to loss of aflatoxin production. *Fungal Biol.* **2012**, *116*, 298−307.

(6) Duran, R. M.; Cary, J. W.; Calvo, A. M. Production of cyclopiazonic acid, aflatrem, and aflatoxin by *Aspergillus flavus* is regulated by *veA*, a gene necessary for sclerotial formation. *Appl. Microbiol. Biotechnol.* **2007**, *73*, 1158−1168.

(7) Yang, G.; Cao, X.; Qin, L.; Yan, L.; Hong, R.; Yuan, J.; Wang, S. Ssu72 Regulates Fungal Development, Aflatoxin Biosynthesis and Pathogenicity in *Aspergillus flavus*. *Toxins* **2020**, *12*, No. 717.

(8) Zhu, Z.; Yang, M.; Bai, Y.; Ge, F.; Wang, S. Antioxidant-related catalase CTA1 regulates development, aflatoxin biosynthesis, and virulence in pathogenic fungus *Aspergillus flavus*. *Environ. Microbiol.* **2020**, *22*, 2792−2810.

(9) Jermnak, U.; Yoshinari, T.; Sugiyama, Y.; Tsuyuki, R.; Nagasawa, H.; Sakuda, S. Isolation of methyl syringate as a specific aflatoxin production inhibitor from the essential oil of Betula alba and aflatoxin production inhibitory activities of its related compounds. *Int. J. Food Microbiol.* **2012**, *153*, 339−344.

(10) Zhou, W.; Hu, L.-B.; Zhao, Y.; Wang, M.-Y.; Zhang, H.; Mo, H.-Z. Inhibition of fungal aflatoxin B1 biosynthesis by diverse

botanically-derived polyphenols. *Trop. J. Pharm. Res.* **2015**, *14*, 605−609.
(11) Moon, Y. S.; Choi, W. S.; Park, E. S.; Bae, I. K.; Choi, S. D.; Paek, O.; Kim, S. H.; Chun, H. S.; Lee, S. E. Antifungal and Antiaflatoxigenic Methylenedioxy-Containing Compounds and Piperine-Like Synthetic Compounds. *Toxins* **2016**, *8*, No. 240.
(12) Dhanamjayulu, P.; Boga, R. B.; Mehta, A. Inhibition of aflatoxin B1 biosynthesis and down regulation of *aflR* and *aflB* genes in presence of benzimidazole derivatives without impairing the growth of *Aspergillus flavus*. *Toxicon* **2019**, *170*, 60−67.
(13) Schultz, D. L.; Luedecke, L. O. Effect of Neutral Fats and Fatty Acids on Aflatoxin Production. *J. Food Prot.* **1977**, *40*, 304−308.
(14) Fanelli, C.; Fabbri, A. A.; Finotti, E.; Passi, S. Stimulation of aflatoxin biosynthesis by lipophilic epoxides. *Microbiology* **1983**, *129*, 1721−1723.
(15) Zhao, X.; Zhi, Q. Q.; Li, J. Y.; Keller, N. P.; He, Z. M. The Antioxidant Gallic Acid Inhibits Aflatoxin Formation in *Aspergillus flavus* by Modulating Transcription Factors FarB and CreA. *Toxins* **2018**, *10*, No. 270.
(16) Lin, J.-Q.; Zhao, X.-X.; Wang, C.-C.; Xie, Y.; Li, G.-H.; He, Z.-M. 5-Azacytidine inhibits aflatoxin biosynthesis in *Aspergillus flavus*. *Ann. Microbiol.* **2013**, *63*, 763−769.
(17) Priyadarshini, E.; Tulpule, P. G. Effect of free fatty acids on aflatoxin production in a synthetic medium. *Food Cosmet. Toxicol.* **1980**, *18*, 367−369.
(18) Burow, G. B.; Nesbitt, T. C.; Dunlap, J.; Keller, N. P. Seed lipoxygenase products modulate *Aspergillus* mycotoxin biosynthesis. *Mol. Plant−Microbe Interact.* **1997**, *10*, 380−387.
(19) Yan, S.; Liang, Y.; Zhang, J.; Chen, Z.; Liu, C. M. Autoxidated linolenic acid inhibits aflatoxin biosynthesis in *Aspergillus flavus* via oxylipin species. *Fungal Genet. Biol.* **2015**, *81*, 229−237.
(20) Affeldt, K. J.; Carrig, J.; Amare, M.; Keller, N. P. Global survey of canonical *Aspergillus flavus* G protein-coupled receptors. *mBio* **2014**, *5*, No. e01501-14.
(21) Brodhagen, M.; Keller, N. P. Signalling pathways connecting mycotoxin production and sporulation. *Mol. Plant Pathol.* **2006**, *7*, 285−301.
(22) Yan, S.; Liang, Y.; Zhang, J.; Liu, C. M. *Aspergillus flavus* grown in peptone as the carbon source exhibits spore density- and peptone concentration-dependent aflatoxin biosynthesis. *BMC Microbiol.* **2012**, *12*, No. 106.
(23) Khalid, S.; Baccile, J. A.; Spraker, J. E.; Tannous, J.; Imran, M.; Schroeder, F. C.; Keller, N. P. NRPS-derived isoquinolines and lipopetides mediate antagonism between plant pathogenic fungi and bacteria. *ACS Chem. Biol.* **2018**, *13*, 171−179.
(24) Ávila, C.; Pelissari, C.; Sezerino, P. H.; Sgroi, M.; Roccaro, P.; Garcia, J. Enhancement of total nitrogen removal through effluent recirculation and fate of PPCPs in a hybrid constructed wetland system treating urban wastewater. *Sci. Total Environ.* **2017**, *584−585*, 414−425.
(25) Bray, D.Critical Point Drying of Biological Specimens for Scanning Electron Microscopy. *Supercritical Fluid Methods and Protocols*; Humana Press, 2000; pp 235−243.
(26) Bolger, A. M.; Lohse, M.; Usadel, B. Trimmomatic: a flexible trimmer for Illumina sequence data. *Bioinformatics* **2014**, *30*, 2114−2120.
(27) Langmead, B.; Trapnell, C.; Pop, M.; Salzberg, S. L. Ultrafast and memory-efficient alignment of short DNA sequences to the human genome. *Genome Biol.* **2009**, *10*, No. R25.
(28) Trapnell, C.; Pachter, L.; Salzberg, S. L. TopHat: discovering splice junctions with RNA-Seq. *Bioinformatics* **2009**, *25*, 1105−1111.
(29) Yanai, I.; Benjamin, H.; Shmoish, M.; Chalifa-Caspi, V.; Shklar, M.; Ophir, R.; Bar-Even, A.; Horn-Saban, S.; Safran, M.; Domany, E.; et al. Genome-wide midrange transcription profiles reveal expression level relationships in human tissue specification. *Bioinformatics* **2005**, *21*, 650−659.
(30) Yan, S.; Zhu, C.; Yu, T.; Huang, W.; Huang, J.; Kong, Q.; Shi, J.; Chen, Z.; Liu, Q.; Wang, S.; et al. Studying the Differences of Bacterial Metabolome and Microbiome in the Colon between Landrace and Meihua Piglets. *Front. Microbiol.* **2017**, *8*, No. 1812.
(31) Yan, S.; Huang, W.; Gao, J.; Fu, H.; Liu, J. Comparative metabolomic analysis of seed metabolites associated with seed storability in rice (*Oryza sativa* L.) during natural aging. *Plant Physiol. Biochem.* **2018**, *127*, 590−598.
(32) Yan, S.; Liu, Q.; Naake, T.; Huang, W.; Chen, M.; Kong, Q.; Zhang, S.; Li, W.; Li, X.; Liu, Q.; et al. OsGF14b modulates defense signaling pathways in rice panicle blast response. *Crop J.* **2021**, *9*, 725−738.
(33) Carberry, S.; Neville, C. M.; Kavanagh, K. A.; Doyle, S. Analysis of major intracellular proteins of *Aspergillus fumigatus* by MALDI mass spectrometry: identification and characterisation of an elongation factor 1B protein with glutathione transferase activity. *Biochem. Biophys. Res. Commun.* **2006**, *341*, 1096−1104.
(34) Heng, Z.; Sheng, O.; Huang, W.; Zhang, S.; Fernie, A. R.; Motorykin, I.; Kong, Q.; Yi, G.; Yan, S. Integrated proteomic and metabolomic analysis suggests high rates of glycolysis are likely required to support high carotenoid accumulation in banana pulp. *Food Chem.* **2019**, *297*, No. 125016.
(35) Schopper, S.; Kahraman, A.; Leuenberger, P.; Feng, Y.; Piazza, I.; Muller, O.; Boersema, P. J.; Picotti, P. Measuring protein structural changes on a proteome-wide scale using limited proteolysis-coupled mass spectrometry. *Nat. Protoc.* **2017**, *12*, 2391−2410.
(36) Franken, H.; Mathieson, T.; Childs, D.; Sweetman, G. M.; Werner, T.; Togel, I.; Doce, C.; Gade, S.; Bantscheff, M.; Drewes, G.; et al. Thermal proteome profiling for unbiased identification of direct and indirect drug targets using multiplexed quantitative mass spectrometry. *Nat. Protoc.* **2015**, *10*, 1567−1593.
(37) Livak, K. J.; Schmittgen, T. D. Analysis of relative gene expression data using real-time quantitative PCR and the 2(-Delta Delta C(T)) Method. *Methods* **2001**, *25*, 402−408.
(38) Huege, J.; Goetze, J.; Dethloff, F.; Junker, B.; Kopka, J. Quantification of stable isotope label in metabolites via mass spectrometry. *Methods Mol. Biol.* **2014**, *1056*, 213−223.
(39) Cerqueira, G. C.; Arnaud, M. B.; Inglis, D. O.; Skrzypek, M. S.; Binkley, G.; Simison, M.; Miyasato, S. R.; Binkley, J.; Orvis, J.; Shah, P.; et al. The *Aspergillus* Genome Database: multispecies curation and incorporation of RNA-Seq data to improve structural gene annotations. *Nucleic Acids Res.* **2014**, *42*, D705−D710.
(40) Li, L.; Stoeckert, C. J., Jr.; Roos, D. S. OrthoMCL: identification of ortholog groups for eukaryotic genomes. *Genome Res.* **2003**, *13*, 2178−2189.
(41) Kumar, S.; Nei, M.; Dudley, J.; Tamura, K. MEGA: a biologist-centric software for evolutionary analysis of DNA and protein sequences. *Briefings Bioinf.* **2008**, *9*, 299−306.
(42) Nielsen, R.; Yang, Z. Likelihood models for detecting positively selected amino acid sites and applications to the HIV-1 envelope gene. *Genetics* **1998**, *148*, 929−936.
(43) Zhang, J.; Nielsen, R.; Yang, Z. Evaluation of an Improved Branch-Site Likelihood Method for Detecting Positive Selection at the Molecular Level. *Mol. Biol. Evol.* **2005**, *22*, 2472−2479.
(44) Yang, Z.; Nielsen, R. Codon-substitution models for detecting molecular adaptation at individual sites along specific lineages. *Mol. Biol. Evol.* **2002**, *19*, 908−917.
(45) Jumper, J.; Evans, R.; Pritzel, A.; Green, T.; Figurnov, M.; Ronneberger, O.; Tunyasuvunakool, K.; Bates, R.; Zidek, A.; Potapenko, A.; et al. Highly accurate protein structure prediction with AlphaFold. *Nature* **2021**, *596*, 583−589.
(46) Mirdita, M.; Schutze, K.; Moriwaki, Y.; Heo, L.; Ovchinnikov, S.; Steinegger, M. ColabFold: making protein folding accessible to all. *Nat. Methods* **2022**, *19*, 679−682.
(47) Jo, S.; Kim, T.; Iyer, V. G.; Im, W. CHARMM-GUI: a web-based graphical user interface for CHARMM. *J. Comput. Chem.* **2008**, *29*, 1859−1865.
(48) Kandt, C.; Ash, W. L.; Tieleman, D. P. Setting up and running molecular dynamics simulations of membrane proteins. *Methods* **2007**, *41*, 475−488.

https://doi.org/10.1021/acs.jafc.2c06230
J. Agric. Food Chem. XXXX, XXX, XXX−XXX

(49) Abraham, M. J.; Murtola, T.; Schulz, R.; Páll, S.; Smith, J. C.; Hess, B.; Lindahl, E. GROMACS: High performance molecular simulations through multi-level parallelism from laptops to supercomputers. *SoftwareX* **2015**, *1*−*2*, 19−25.
(50) Huang, J.; Rauscher, S.; Nawrocki, G.; Ran, T.; Feig, M.; de Groot, B. L.; Grubmuller, H.; MacKerell, A. D., Jr. CHARMM36m: an improved force field for folded and intrinsically disordered proteins. *Nat. Methods* **2017**, *14*, 71−73.
(51) Vanommeslaeghe, K.; Hatcher, E.; Acharya, C.; Kundu, S.; Zhong, S.; Shim, J.; Darian, E.; Guvench, O.; Lopes, P.; Vorobyov, I.; et al. CHARMM general force field: A force field for drug-like molecules compatible with the CHARMM all-atom additive biological force fields. *J. Comput. Chem.* **2010**, *31*, 671−690.
(52) Deift, P.; Zhou, X. A steepest descent method for oscillatory Riemann−Hilbert problems. Asymptotics for the MKdV equation. *Ann. Math.* **1993**, *137*, 295−368.
(53) Parrinello, M.; Rahman, A. Crystal structure and pair potentials: A molecular-dynamics study. *Phys. Rev. Lett.* **1980**, *45*, 1196.
(54) Hoover, W. G. Canonical dynamics: Equilibrium phase-space distributions. *Phys. Rev. A* **1985**, *31*, 1695−1697.
(55) Hess, B.; Bekker, H.; Berendsen, H. J.; Fraaije, J. G. LINCS: a linear constraint solver for molecular simulations. *J. Comput. Chem.* **1997**, *18*, 1463−1472.
(56) Essmann, U.; Perera, L.; Berkowitz, M. L.; Darden, T.; Lee, H.; Pedersen, L. G. A smooth particle mesh Ewald method. *J. Chem. Phys.* **1995**, *103*, 8577−8593.
(57) Michaud-Agrawal, N.; Denning, E. J.; Woolf, T. B.; Beckstein, O. MDAnalysis: a toolkit for the analysis of molecular dynamics simulations. *J. Comput. Chem.* **2011**, *32*, 2319−2327.
(58) McGibbon, R. T.; Beauchamp, K. A.; Harrigan, M. P.; Klein, C.; Swails, J. M.; Hernandez, C. X.; Schwantes, C. R.; Wang, L. P.; Lane, T. J.; Pande, V. S. MDTraj: A Modern Open Library for the Analysis of Molecular Dynamics Trajectories. *Biophys. J.* **2015**, *109*, 1528−1532.
(59) Kong, Q.; Chang, P. K.; Li, C.; Hu, Z.; Zheng, M.; Sun, Q.; Shan, S. Identification of AflR Binding Sites in the Genome of *Aspergillus flavus* by ChIP-Seq. *J. Fungi* **2020**, *6*, No. 52.
(60) Humphrey, W.; Dalke, A.; Schulten, K. VMD: visual molecular dynamics. *J. Mol. Graphics* **1996**, *14*, 33−38.
(61) Payne, G. A.; Nierman, W. C.; Wortman, J. R.; Pritchard, B. L.; Brown, D.; Dean, R. A.; Bhatnagar, D.; Cleveland, T. E.; Machida, M.; Yu, J. Whole genome comparison of *Aspergillus flavus* and *A. oryzae*. *Med. Mycol.* **2006**, *44*, S9−S11.
(62) Gibbons, J. G.; Salichos, L.; Slot, J. C.; Rinker, D. C.; McGary, K. L.; King, J. G.; Klich, M. A.; Tabb, D. L.; McDonald, W. H.; Rokas, A. The evolutionary imprint of domestication on genome variation and function of the filamentous fungus *Aspergillus oryzae*. *Curr. Biol.* **2012**, *22*, 1403−1409.
(63) Hollingsworth, S. A.; Dror, R. O. Molecular Dynamics Simulation for All. *Neuron* **2018**, *99*, 1129−1143.
(64) Kokh, D. B.; Doser, B.; Richter, S.; Ormersbach, F.; Cheng, X.; Wade, R. C. A workflow for exploring ligand dissociation from a macromolecule: Efficient random acceleration molecular dynamics simulation and interaction fingerprint analysis of ligand trajectories. *J. Chem. Phys.* **2020**, *153*, No. 125102.
(65) Szklarczyk, D.; Gable, A. L.; Lyon, D.; Junge, A.; Wyder, S.; Huerta-Cepas, J.; Simonovic, M.; Doncheva, N. T.; Morris, J. H.; Bork, P.; et al. STRING v11: protein-protein association networks with increased coverage, supporting functional discovery in genome-wide experimental datasets. *Nucleic Acids Res.* **2019**, *47*, D607−D613.
(66) Adhikari, H.; Cullen, P. J. Role of phosphatidylinositol phosphate signaling in the regulation of the filamentous-growth mitogen-activated protein kinase pathway. *Eukaryotic Cell* **2015**, *14*, 427−440.
(67) Ghugtyal, V.; Garcia-Rodas, R.; Seminara, A.; Schaub, S.; Bassilana, M.; Arkowitz, R. A. Phosphatidylinositol-4-phosphate-dependent membrane traffic is critical for fungal filamentous growth. *Proc. Natl. Acad. Sci. U.S.A.* **2015**, *112*, 8644−8649.
(68) Weydert, C. J.; Cullen, J. J. Measurement of superoxide dismutase, catalase and glutathione peroxidase in cultured cells and tissue. *Nat. Protoc.* **2010**, *5*, 51−66.
(69) Caceres, I.; El Khoury, R.; Bailly, S.; Oswald, I. P.; Puel, O.; Bailly, J. D. Piperine inhibits aflatoxin B1 production in *Aspergillus flavus* by modulating fungal oxidative stress response. *Fungal Genet. Biol.* **2017**, *107*, 77−85.
(70) Yang, M.; Lu, L.; Li, S.; Zhang, J.; Li, Z.; Wu, S.; Guo, Q.; Liu, H.; Wang, C. Transcriptomic insights into benzenamine effects on the development, aflatoxin biosynthesis, and virulence of *Aspergillus flavus*. *Toxins* **2019**, *11*, No. 70.
(71) Li, X. M.; Li, Z. Y.; Wang, Y. D.; Wang, J. Q.; Yang, P. L. Quercetin Inhibits the Proliferation and Aflatoxins Biosynthesis of *Aspergillus flavus*. *Toxins* **2019**, *11*, No. 154.
(72) Falade, T. D. O.; Chrysanthopoulos, P. K.; Hodson, M. P.; Sultanbawa, Y.; Fletcher, M.; Darnell, R.; Korie, S.; Fox, G. Metabolites Identified during Varied Doses of *Aspergillus* Species in *Zea mays* Grains, and Their Correlation with Aflatoxin Levels. *Toxins* **2018**, *10*, No. 187.
(73) Fountain, J. C.; Koh, J.; Yang, L.; Pandey, M. K.; Nayak, S. N.; Bajaj, P.; Zhuang, W. J.; Chen, Z. Y.; Kemerait, R. C.; Lee, R. D.; et al. Proteome analysis of *Aspergillus flavus* isolate-specific responses to oxidative stress in relationship to aflatoxin production capability. *Sci. Rep.* **2018**, *8*, No. 3430.
(74) Yang, K.; Geng, Q.; Song, F.; He, X.; Hu, T.; Wang, S.; Tian, J. Transcriptome Sequencing Revealed an Inhibitory Mechanism of *Aspergillus flavus* Asexual Development and Aflatoxin Metabolism by Soy-Fermenting Non-Aflatoxigenic *Aspergillus*. *Int. J. Mol. Sci.* **2020**, *21*, No. 6994.
(75) Pan, L.; Chang, P.; Jin, J.; Yang, Q.; Xing, F. Dimethylformamide Inhibits Fungal Growth and Aflatoxin B1 Biosynthesis in *Aspergillus flavus* by Down-Regulating Glucose Metabolism and Amino Acid Biosynthesis. *Toxins* **2020**, *12*, No. 683.
(76) Cary, J. W.; Gilbert, M. K.; Lebar, M. D.; Majumdar, R.; Calvo, A. M. *Aspergillus flavus* Secondary Metabolites: More than Just Aflatoxins. *Food Saf.* **2018**, *6*, 7−32.
(77) Xie, H.; Jallow, A.; Yue, X.; Wang, X.; Fu, J.; Mwakinyali, S. E.; Zhang, Q.; Li, P. *Aspergillus flavus*'s Response to Antagonism Bacterial Stress Sheds Light on a Regulation and Metabolic Trade-Off Mechanism for Adversity Survival. *J. Agric. Food Chem.* **2021**, *69*, 4840−4848.
(78) Hong, S. Y.; Roze, L. V.; Linz, J. E. Oxidative stress-related transcription factors in the regulation of secondary metabolism. *Toxins* **2013**, *5*, 683−702.
(79) Hong, S. Y.; Roze, L. V.; Wee, J.; Linz, J. E. Evidence that a transcription factor regulatory network coordinates oxidative stress response and secondary metabolism in *aspergilli*. *MicrobiologyOpen* **2013**, *2*, 144−160.
(80) Roze, L.; Laivenieks, M.; Hong, S. Y.; Wee, J.; Wong, S. S.; Vanos, B.; Awad, D.; Ehrlich, K.; Linz, J. Aflatoxin Biosynthesis Is a Novel Source of Reactive Oxygen Species-A Potential Redox Signal to Initiate Resistance to Oxidative Stress? *Toxins* **2015**, *7*, 1411−1430.
(81) Sweany, R. R.; Mack, B. M.; Moore, G. G.; Gilbert, M. K.; Cary, J. W.; Lebar, M. D.; Rajasekaran, K.; Damann, K. E., Jr. Genetic Responses and Aflatoxin Inhibition during Co-Culture of Aflatoxigenic and Non-Aflatoxigenic *Aspergillus flavus*. *Toxins* **2021**, *13*, No. 794.
(82) Chang, P. K.; Scharfenstein, L. L.; Luo, M.; Mahoney, N.; Molyneux, R. J.; Yu, J.; Brown, R. L.; Campbell, B. C. Loss of *msnA*, a putative stress regulatory gene, in *Aspergillus parasiticus* and *Aspergillus flavus* increased production of conidia, aflatoxins and kojic acid. *Toxins* **2011**, *3*, 82−104.
(83) Fountain, J. C.; Bajaj, P.; Pandey, M.; Nayak, S. N.; Yang, L.; Kumar, V.; Jayale, A. S.; Chitikineni, A.; Zhuang, W.; Scully, B. T.; et al. Oxidative stress and carbon metabolism influence *Aspergillus flavus* transcriptome composition and secondary metabolite production. *Sci. Rep.* **2016**, *6*, No. 38747.
(84) Zhang, J. D.; Han, L.; Yan, S.; Liu, C. M. The non-metabolizable glucose analog D-glucal inhibits aflatoxin biosynthesis

https://doi.org/10.1021/acs.jafc.2c06230
J. Agric. Food Chem. XXXX, XXX, XXX−XXX

and promotes kojic acid production in *Aspergillus flavus*. *BMC Microbiol.* **2014**, *14*, No. 95.
(85) Tian, F.; Lee, S. Y.; Woo, S. Y.; Choi, H. Y.; Heo, S.; Nah, G.; Chun, H. S. Transcriptomic responses of *Aspergillus flavus* to temperature and oxidative stresses during aflatoxin production. *Sci. Rep.* **2021**, *11*, No. 2803.
(86) Roze, L. V.; Chanda, A.; Linz, J. E. Compartmentalization and molecular traffic in secondary metabolism: a new understanding of established cellular processes. *Fungal Genet. Biol.* **2011**, *48*, 35−48.

https://doi.org/10.1021/acs.jafc.2c06230
J. Agric. Food Chem. XXXX, XXX, XXX−XXX